DC Solid State Circuit Breaker for AEA

Bachelor Graduation Thesis Group K

14/06/2024

This thesis has been prepared with contributions from:

Project members:

Maya Peeters	5260469
David van Beelen	4602846
Jorrit van Drie	5176506

Under the supervision of:
Mohamad Ghaffarian Niasar
Jianning Dong
Amir Heidary

Thesis committee members:
Mohamad Ghaffarian Niasar
Jianning Dong
Amir Heidary
Marjan Popov

DELFT UNIVERSITY OF TECHNOLOGY

FACULTY OF ELECTRICAL ENGINEERING, MATHEMATICS AND COMPUTER SCIENCE

ELECTRICAL ENGINEERING PROGRAMME

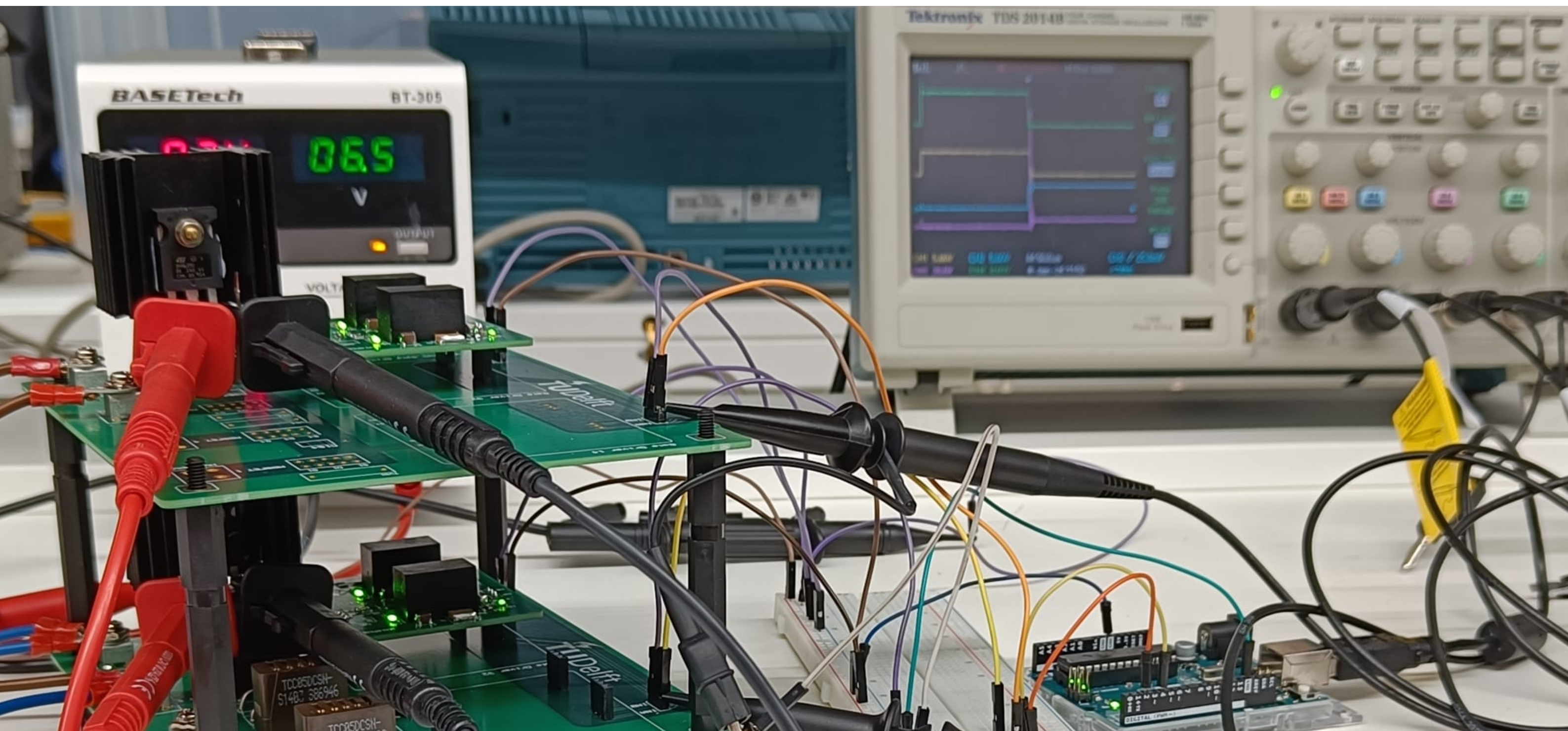

Acknowledgements

First of all we want to thank our supervisors, Mohamad Ghaffarian Niasar and Jianning Dong for making us realize how much we do not know yet about Electrical Engineering, giving us personal lectures and helping us every week to get the results. We want to thank Amir Heidary for his time, help, enthusiasm and extremely useful knowledge about circuit breakers. Our thanks also go out to Jundong Wang, Weichuan Zhao and all other PhD students that helped us with both practical and theoretical insights to realise our project. We want to thank the staff of the high voltage lab that kept an eye on us so we would not break ourselves or their equipment during testing. Next we want to thank the more personal support during this period. Thank you, to our family and girlfriends for the support, love and patience when we bored you with our thesis.

For Arie, my dear father, whom I wish could have read this.

Abstract

As the need for both clean electricity and reduction of carbon emission rises, all-electric airplanes have the potential to reshape the field of aviational transport to fit this need. The development of such airplanes necessitates the advancement of highly reliable and efficient electrical systems, among which circuit breakers play a critical role. This paper investigates design considerations and challenges associated with circuit breakers for all-electric aircraft. The study explores possible circuit topologies that are capable to interrupt a 3 kV and 500 A power flow when a fault in the system causes a short circuit. Through simulations and experimental validations, the paper aims to propose an optimised circuit breaker design that enables reliable electric power systems in all-electric aircraft.

Contents

Chapter 1

Introduction

In today's society one of the biggest problems faced is global warming. Climate change causes immense problems to our ecosystems and causes natural disasters to occur around communities all around the world. To face this problem the entire world is trying to switch to renewable and sustainable energy sources for all our electricity. While the grid is already being fed partially by renewable energy sources to reduce carbon emission, there are still many fields where real improvements can be made. One of these is transportation, especially air travel. Yearly 1.5 billion tons of CO_2 is produced which is 2.1% of global CO_2 emissions. Nowadays, engines fueled by kerosene are used within an aircraft, which cause this share of emissions [1]. To try and counter these emissions it is good to consider an electric aircraft, whereby air travel can adapt the use of an electric micro grids instead of large polluting motors. One of the biggest challenges about realizing an electric aircraft is the propulsion system for the flight, and especially the takeoff since it requires the most power. Producing enough thrusting power using just electricity will require immense high current and voltage ratings that are hard to both control and keep safe.

Figure 1.1: A conceptualisation of an all-electric-aircraft from Elysian [2].

1.1 All Electric Aircraft

An aircraft in which every component is driven by electricity is called an all electric aircraft (AEA), such as the one shown in Figure 1.1. The big challenge with realising an AEA is creating a reliable, safe and efficient grid architecture, like the one shown in Figure 1.2. This architecture should be designed for the

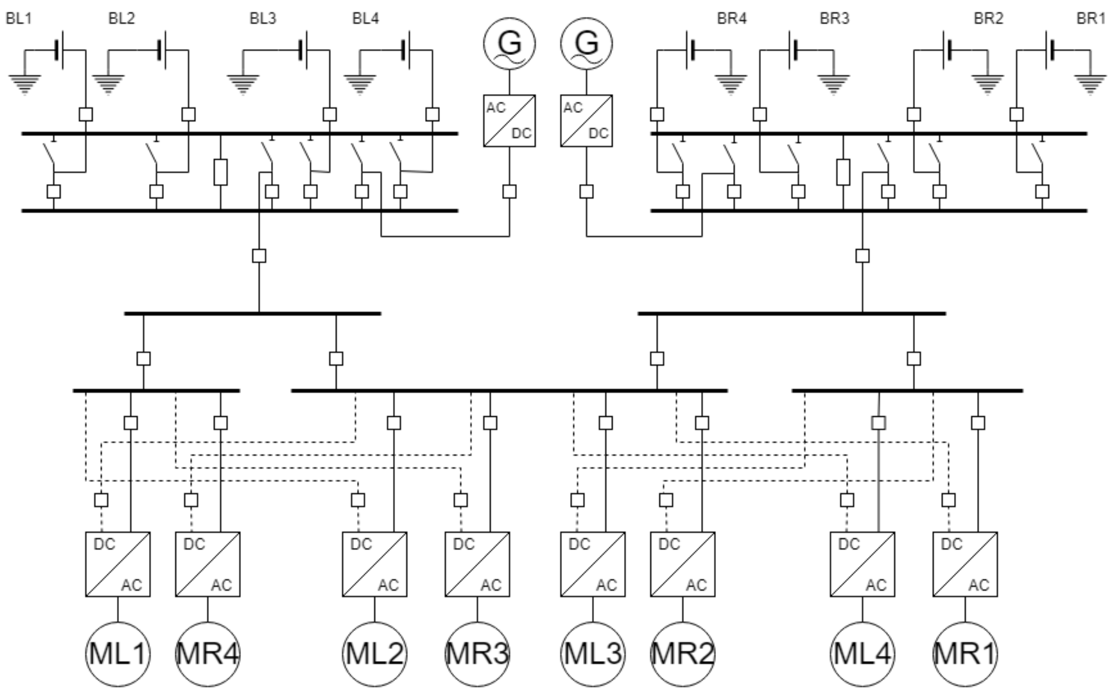

Figure 1.2: Topology of a High Voltage DC grid architecture with 8 battery packs. Where every circuit breaker is marked as a white square. ML and MR mean Motor Left and Motor Right respectively. The thicker lines are bus-bars and are at the top connected with bus couplers. There are two generators denoted by 'G'. [3]

high power consumption during take off, it should be able to withstand the extreme conditions in which a plane might fly, it should deal with the high temperatures that are created with these kinds of powers and most important of all it needs to be safe.
The reliability of its subsystem is paramount when creating safety in an electric grid. It is inevitable that something is going to fail, so it is necessary that this is handled and that a single failure does not lead to catastrophic situations. A useful way to handle potential faults is a circuit breaker.

1.2 Circuit breaker

Circuit breakers are used to disconnect a load from the system when a part of the circuit is overloaded such that the rest of the system is not affected by that fault. These faults include short circuit currents and over-current. Due to the high power requirements of an electric aircraft, this paper especially considers short-circuit currents as these can reach very high values. Furthermore the focus will lie on solid state circuit breakers (SSCB) as these circuit breakers are light in weight and have fast reaction time which are important characteristics for in an aircraft.

In order to get an understanding of a circuit breaker an IGBT switch connected to a load was modeled in Simulink. The rated nominal voltage and current within an aircraft is taken to be 3 kV and 500 A. This is simulated by making the source voltage 3 kV and the load resistance 6 Ω. Furthermore, the line impedance of $3 \cdot 10^{-3} + 2 \cdot 10^{-5} j\omega\,\Omega$ and a source impedance of $1 \cdot 10^{-3} + 1 \cdot 10^{-5} j\omega\,\Omega$ is modeled using a resistor and inductor. Lastly the fault current is produced at time t = $5 \cdot 10^{-3}$ s by reducing the resistor to 0.001 Ω. The signal provided to the switch is a simple step function which provides a 1 until $5.5 \cdot 10{-}3$ s, then it provides a 0. The extra 0.5 ms is the delay for detecting the fault and response of the switch. The setup of this simulation can be seen in figure 1.3. The voltage is measured across the switch and the current is measured before the switch.

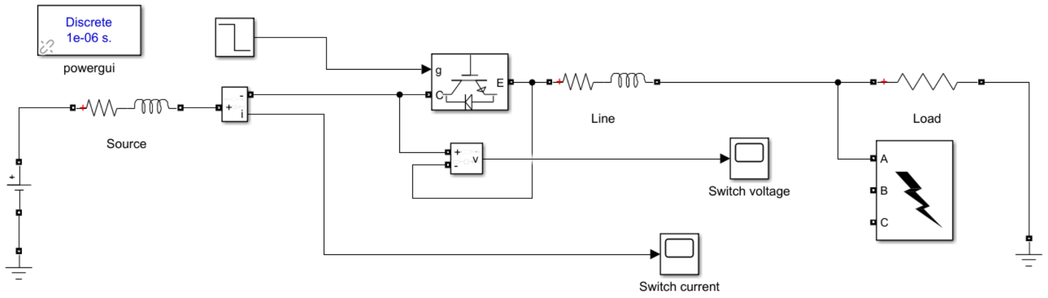

Figure 1.3: The simulation setup for 3 (kV) and 500 (A) nominal rating

The setup was simulated, the voltage over the switch and the current through the switch were measured and plotted. These results can be seen in figure 1.4. As expected the current starts at 500 A which is the nominal rated current through the system and ends at 0 A after the fault. The fault occurs at 0.005 s, which is seen by the steep increase in current. After 0.5 ms the switch reacts and turns of the system which sets the current to 0 A. The current is at $4.8 \cdot 10^4$ A once the switch is turned off. Due to the high current and the sudden disconnect of the circuit a high voltage drop is created over the switch. From the simulation it can be seen that this voltage spike reaches $1.443 \cdot 10^6$ V. A few conclusions can be drawn from this simulation. Firstly, the current and voltage are too high for the switch to handle. This means that overcurrent and overvoltage suppression is needed. Secondly it can be seen from Figure 1.4 that a faster response time will lead to a lower fault current. A combination between a fast response time and correct voltage and current suppression is therefore needed to reduce the overvoltage and overcurrent on the switch such that it does not break.

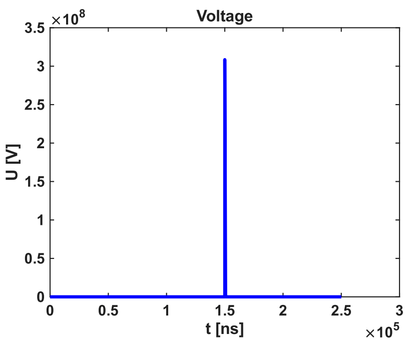

(a) Voltage behaviour over a switch as circuit breaker without protection

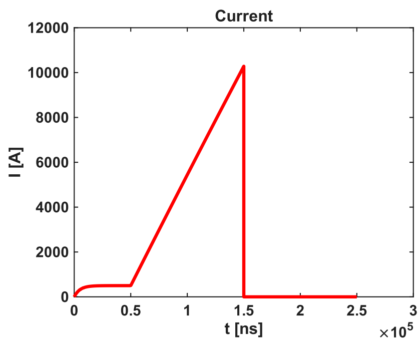

(b) Current behaviour through a switch as circuit breaker without protection

Figure 1.4: Voltage and current behaviour of a switch as circuit breaker without protection

1.3 Project goal

The goal of this research is to find a highly reliable and lightweight circuit breaker that is suitable for aviational use. In this paper a design for a unidirectional DC SSCB with current limiter and voltage suppressor circuit is proposed, analysed and tested. The goal is to specifically analyse the mass, reliability and feasibility of this component for in an all electric aircraft.

1.4 Thesis outline

This thesis will start with an explanation of what the proposed circuit breaker for an all electric aircraft should have in terms of specifications in Chapter 2. Next a selection of different circuit breakers will be explained to show what the possibilities are in this field in Chapter 3. After this the choices made for the proposed circuit breaker are explained and justified in Chapter 4. Then the simulations of the proposed circuit breaker in full-scale operating conditions are shown. The circuit breaker will be simulated using different component values. This is explained in chapter 5. This papers optimizes the weight of the breaker by using equations designed to estimate the weight of the components that are used. These equations are explained in Chapter 6. The equations will be used in an optimisation algorithm, which is explained and shown in Chapter 7, to derive the final values for the components of the breaker. Finally the final design used is shown in Chapter 8, and the testing of a downscaled version is explained and the results are shown in Chapter 9. The reliability of the breaker is calculated in Chapter 10 and the findings in this paper will be concluded and discussed in Chapter 11.

Chapter 2

Specification

The circuit breaker should satisfy the following conditions, which form the basis of the parameters for the optimization algorithm and further choices:

- Nominal voltage 3 kV
- Nominal current 500 A
- Weight under 15 kg
- Fault interruption at a maximum of 1500 A
- Fault voltage up to 3.6 kV
- Duration of peak current maximally 1 ms

There are several different places within the aircraft where the breaker requires to operate within different nominal voltages and currents. The circuit breaker proposed in this thesis is designed to be placed near one of the batteries or cables to the motor for which the nominal current and voltage is specified to be 500 A and 3 kV respectively. The weight of the breaker is ideally as low as possible, but a maximum limit is set to 15 kg per breaker. This is based on a restriction on the total weight of the aircraft which was considered through a reliability analysis done in the paper "Design & Reliability Assessment of AEA Propulsion Grid".

Based on the nominal voltage a peak voltage of a factor 1.2 larger was chosen, this is 3.6 kV. For the switch a derating of 60% was taken into account. This derating is due to the high altitude at which the aircraft flies. Considering an aircraft that can fly at a height of 5.8 km the derating factor will be 0.6 [4]. Using this derating factor a switch rated at a voltage of 6kV needs to be selected. This switch is the FZ750R65KE3 from infineon. The important information from the datasheet from this switch can be seen in appendix A.1 [5]. The switch has a voltage rating of 6.5 kV and a nominal current of 750A. According to the specifications this switch can handle the nominal current and also a peak current pulse of 1500 A for a maximum time of 1ms. This is where the further specifications are derived from.

Chapter 3

Topologies

There are many different solid state circuit breaker designs, that include a variety of mechanisms to detect a fault, trigger the switch and protect the switch. In this chapter three circuit breaker designs are discussed and compared to get an understanding of how a circuit breaker works. Also the mechanical circuit breaker will be discussed, especially why it is not applicable for this project.

3.1 Z-source circuit breaker

A Z-source circuit breaker is a breaker that uses the principle of a z-source inverter which converts DC current to AC. The advantage of the breaker is that it can auto-detect the fault. Therefore a fault detection system is not needed. In order to auto detect the fault, thyristors are used as switch. The conventional z-source circuit breaker has an inductor placed in the return path, which prevents a common ground. There have however been many adaptations to the conventional z-source breaker such that the inductor is not in the return path. One of the adaptations is proposed in [6]. The design for this breaker is shown in figure 3.1a.

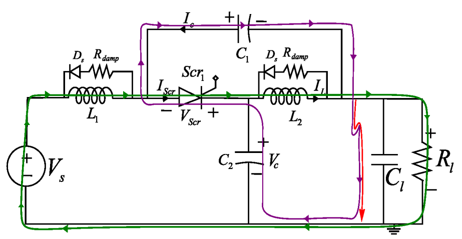

(a) Circuit diagram of the Z-SSCB circuit breaker [6]

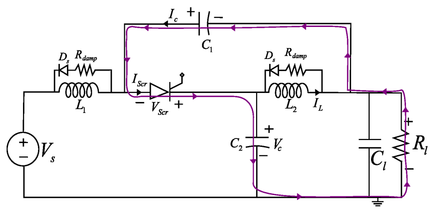

(b) Circuit diagram of the reverse current through the Z-source breaker [6]

In normal operating conditions the current flows through L_1, L_2 and SCR_1, while capacitor C_2 is charged and C_1 discharged. This can be seen by the green line in figure 3.1a. If a short circuit occurs before the load (shown by the red line in figure 3.1a), C_2 will discharge in the opposite direction of the main current. Since the discharge is almost instant and thus can be seen as a very high frequency. The impedance of an inductor and capacitor are calculated as, $Z = j\omega L$ and $Z = \frac{1}{j\omega C}$ respectively. When the frequency is very high it means the capacitor becomes a short circuit and the inductor becomes an open circuit, causing the capacitor to discharge through the capacitor. The discharge current of C_2 flows through C_2, SCR_1 and C_1, shown by the purple line in figure 3.1a. This causes SCR_1 to go into the off-state. After the fault C_1 is now charged and C_2 discharged. The circuit breaker is closed again by turning the thyristor on. This leads to C_1 discharging through the load, creating a negative current through the load, this is shown in figure 3.1b. This is undesirable for an electric aircraft, as these loads consists of among other things, the motors, which deteriorate over time when exposed to a negative current. Furthermore, a negative current flowing through a DC motor can introduce a sudden surge. Therefore, a z-source circuit breaker is not fitting for the application within an electric aircraft. Luckily adaptations have been made to the z-source topology to prevent negative current flowing through the load. One of a common re-occurring topology is the Modular bi-directional circuit breaker.

3.2 Modular bidirectional circuit breaker

Bidirectional circuit breakers can handle power flow in both directions. Therefore, they can also protect a system from faults in either direction. The modular aspect ensures that the ratings for each module can be lower, thus the components do not need immense ratings and are more readily available. Additionally the modular aspects makes the system "plug-and-play" which makes for flexibility during maintenance [7]. The modular bidirectional circuit breaker design proposed in [7] is illustrated in Figure 3.2.

This topology works by always having a capacitor charged. This is done by sending a pulse once in a while to thyristor T1. When the capacitor is fully charged the thyristor automatically turns off by the negative current through it. When a fault occurs, the capacitor discharges which results in a current through L2, this induces a current through L1 due to the coupling. This current should be opposite to the fault current and negate this current fully.

The downside of this design is mainly its complexity since thyristors need a negative current to switch to the OFF-state. Here it is done with a capacitor and coupled inductors, adding these extra components adds weight and makes the full design quite heavy in a full scaled circuit breaker.

The thyristors all need the correct ratings and they can become heavy when dealing with these magnitudes of voltages. Having 5 in just one circuit breaker makes it unsuitable for the application of this paper.

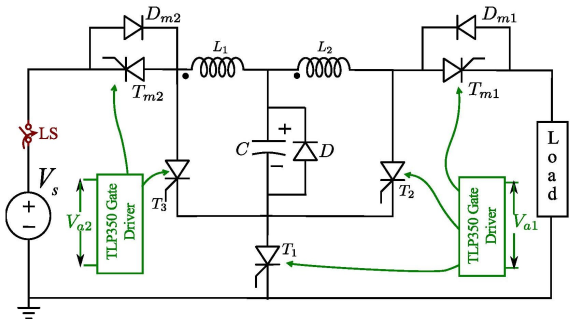

Figure 3.2: A proposed modular design for bidirectional solid-state circuit breakers [7]

3.3 Bidirectional SSCB with snubber circuit

Unlike the other two topologies discussed above, this topology does not use thyristors. This drastically changes the topology as now the switch is not triggered by a zero crossing current, but by a signal sent to the gate of the MOSFET. As mentioned before in the introduction, disconnecting the system suddenly will cause a peak in the voltage across the switch and the current through it. These peaks are restricted due to the snubber circuit, MOV and current limiting inductor placed around and before the switch. When the switch opens, the capacitor fills and the current commutes to the MOV, suppressing the voltage. The inductor further limits the rise of current as it is dependent on $\frac{di}{dt}$. This design is more reliable than the previous designs due to its simplicity. It does not require the production of a negative crossing current to open the switch and instead relies on a fault detection system. The system is considered bidirectional as depending on the direction of the current flow it can cross either of the two switches [8].

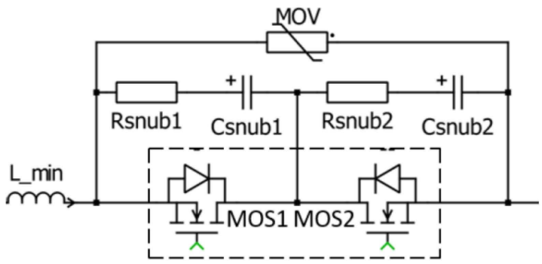

Figure 3.3: Circuit design of a SSCB circuit breaker [8]

Due to the simplicity of the design which implies less components so less losses and higher reliability the bidirection SSCB with snubber circuit and current limiter was decided upon as the basis of the design proposed in this thesis. It is a simple and therefore reliable design and if the correct values are chosen a design powerful enough for in an electric aircraft.

3.4 Mechanical circuit breaker

In a mechanical circuit breaker, the switch is closed in nominal operation. When a fault occurs the fault will be detected, this can be done using magnetic or thermal detection. When the fault is detected the switch physically opens to stop the circuit. However the current continues to flow. This happens because the overvoltage creates sparks across the opening switch and these sparks become an arc as the current continues to flow. This arc needs to be extinguished by the breaker. When this arc is extinguished the current stops to flow. Different mechanical circuit breakers have different methods of controlling and extinction of the arc [9].
The vacuum interpreter is an example of a mechanical circuit breaker. They can deal with high current up to 63.5 kA at several 10 kV however are not yet applicable for DC as they are not interoperable due to no zero crossing. Furthermore a circuit breaker with an arc chamber is another example of a mechanical circuit breaker. When the circuit breaker is triggered it produces an arc which is driven into the arc chamber. These circuit breakers are geometrically complex and heavy, making them not ideal for in an aircraft [10].

One advantage of a mechanical circuit breaker compared to a solid state circuit breaker is that it has a much lower on-state contact resistance, with SSCB having a resistance of three orders of magnitude larger. This is due to the semiconductors. Having semiconductors with an on-state resistance as small as possible is therefore something that needs to be taken into consideration [10]. Mechanical circuit breakers are not ideal for DC power systems on an aircraft as they are slow, heavy and have an arc-less operation requirement. Furthermore mechanical circuit breakers have moving parts that degrade more quickly over time [11] [12].

Paper [9] compares an SSCB and mechanical circuit breaker in both an over current and short current situation. From the experiments it can be concluded that the SSCB has a much faster operation time in the turn-off condition. This is for a short circuit current around a couple of microseconds for an SSCB while for an mechanical circuit breaker it can be between 0.1-1 s.

The mass of a mechanical circuit breaker is also a large disadvantage, especially within the aircraft, where the mass is important. According to [13] the mass of an SSCB can be between 0.084 and 1.344kg for a voltage range of 2.5 to 40kV and a current range between 280 en 4.48kA. The weight of a mechanical circuit breaker is around 160kg for a current 4.15kA and voltage of 3.6kV. The weight of a mechanical circuit is therefor a hundred times larger which is one of the main drawbacks of using a mechanical circuit breaker for an aircraft. However it must be taken into account that an SSCB often requires a heat sink which is often even larger than the semiconductor itself [14].

Chapter 4

The Unidirectional circuit breaker with snubber and current limiter

The circuit breaker with snubber circuit and current limiter formed the basis of the proposed design in this paper however there were other options of switch, over voltage suppression and over current suppression that were considered. For all three segments there are different components that can be used and these will be discussed in this chapter. The basis of our selection criteria were: weight, reliability and whether it is feasible within the scope of this project. Furthermore the method to detect the fault and send a signal to the switch is also touched upon in this section.

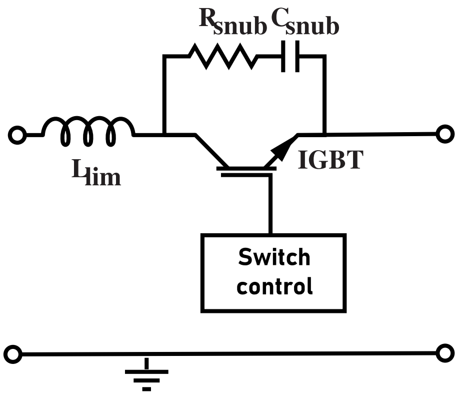

Figure 4.1: The final circuit breaker design of a unidirectional circuit breaker with current limiting inductor and snubber circuit

4.1 Switch

From the topologies mentioned in chapter 3 it was evident that there are three common used switches within SSCB circuit breakers namely: thyrsitors, MOSFETs and IGBTs. These three switches were analysed and compared such that the best switch based on on-state resistance, response time and weight could be selected.

As seen in the first two topologies in Chapter 3 the thyristor is a common used switch within circuit breakers. The benefits of a thyristor for in a SSCB is that it has low ON-state resistance, meaning low losses when turned on and in conducting mode. As it turns off when experiencing a zero or negative signal it is also possible to auto-detect the fault. However this concept is conflicting as this means when a fault current occurs an inverse current needs to be produced to turn of the thyristor rather than sending a signal. The negative current is often produced using charged capacitors and coupled inductors, which leads to leak currents and to extra losses. It additionally leads to the use of extra components which is extra weight for the breaker. Furthermore the thyristor also has a slow response time and is heavy compared to the other switches when dealing with peak voltages in an aircraft, this is further evident from the modular bidirectional circuit breaker design in section 3.2.

Besides thyristors MOSFETs and IGBTs can also be used as switching devices within circuit breakers. MOSFETs are similar switches to IGBTs. Unlinke the thyristor, where a negative current is required to turn off the switch, with these switches the current flow between the source and the drain is manipulated by a voltage applied across the gate and source of the switch. The main trade-off between the two switches is between weight, on-state resistance and switching time. A MOSFET has a much faster switching time than the IGBT, however the IGBT has a much lower on-state resistance. The lower on-state resistance is ideal for high powers as this leads to lower power losses. MOSFETs on-state resistance is susceptible to an increase in power, while IGBTs are less influenced by this. Eventhough the IGBT has slower switching time, due to the lower power losses an IGBT was selected as the switch instead of the MOSFET [15].

4.2 Voltage suppression

This paper discusses three main over-voltage suppression components used in a SSCB, these include TVS, MOVs and snubber circuits. MOVs are metal oxide varistors which is a type of voltage dependent resistor often used with high voltage circuit breakers. While useful, when exposed to high stresses in fault events, the lifespan and reliability degrade significantly over time [16]. DC faults are large currents that rise at high rates, which when happening repeatedly degrades the MOV quickly. Furthermore, preliminary research indicates that the size and weight of MOVs might not be best suitable for this project [17].

A TVS is a transient voltage suppression. These work similar to an avalanche diode but are also applicable for higher voltage ratings. A TVS has higher reliability than MOVs, as it is less susceptible to degradation over time [18]. One disadvantage of the TVS is that it is less applicable for high voltages. Their voltage rating is maximally around 540V, which means series placing of the TVS is required to limit the voltage to rates considered for this breaker. A TVS is therefore not applicable for this project [19]. Instead an RC snubber was considered. It is a reliable component, due to its simplicity, and capability of handling high voltages. An RC snubber consists of a capacitor which limits the rise in voltage and a resistor used to dissipate the excess energy. The RC snubber does have a disadvantage of having current oscillations. This can be solved by placing a diode over the system. This is a design choice that was considered through the project if needed, however the values of the capacitor and resistor were chosen such that the oscillations were not significant, therefore an extra diode (hence extra weight) was not required [20]. A combination of the above mentioned voltage suppression methods was also considered. However to keep the simplicity within the breaker and reduce the weight the choice was made to use as little components as possible.

4.3 Current suppression

This paper considers three main types of current suppression, namely: controlled inductance, uncontrolled inductance and superconductive. Both superconductors and controlled inductors can adapt their resistivity depending on which state they are in. The most common type of superconductor is a resistive superconductor. During normal operation the full current through the system flows through the superconductor, providing a resistance close to $0\,\Omega$. As the current rises and the change of current increases this forces the superconductor out of its superconductive conditions and provides a significant resistance that reduces the current flowing through it [21]. A controlled inductance uses a similar concept. Except instead the inductance of the inductor is changed to limit the overcurrent. The technology for both superconductors and controlled inductances are still being developed and not yet available for testing. Also, these components need to be managed constantly, which adds complexity. Using these components is therefore not feasible for this project and will be left out of the scope of this thesis [22]. Instead an uncontrolled inductor will be used. This is a passive inductor that is placed before the circuit breaker to limit the fault current. The global voltage behaviour of an inductor ($v = L\frac{di}{dt}$) shows that the voltage drop over the inductor is dependent on the change of current through the inductor. The inductor will experience a large change in current when a short circuit fault occurs. This induces a voltage which resists the flow of current.

4.4 Fault detection

When a fault occurs it gets detected by the fault detection mechanism and a signal should be sent to the switch to disconnect. Hence, a subsystem is implemented to detect whether a fault occurs. Unlike the z-source and modular bidirectional circuit breaker, the fault in the proposed topology cannot be auto-detected. This fault detection instead can be done by measuring the current or voltage in the system, or the change in either.

Typical current measuring schemes that were considered for this paper were current transformers, Hall effect sensors, and shunt resistor as well as a coupled inductor for measuring the change in current. As for the voltage measuring, a resistive voltage divider was considered. Because the system has a DC architecture, a current transformer could not be implemented. The Hall effect sensor is more suitable for a DC system such as the one described in this paper. However both voltage and current ratings exceed the typical values of available Hall effect sensors, which tend to measure either voltage or current in the order of magnitude that is relevant to the proposed system. As researching and building a custom application of a Hall effect sensor is outside the scope of this paper, this option was discarded. To use a coupled inductor to measure the change in current already adds to complexity on gauging fault behaviour as a time-derivative signal, but also risks adding too much inductance to the system. Also, operating a coupled inductor at the operation conditions of this system can lead to saturation in the inductors, distorting the sensing behaviour. This is why the coupled inductor was not considered further in this paper. To measure the current via a shunt resistor is straightforward enough to be applied in this system. But this comes at the cost that this resistor dissipates much power when used by itself. Seeing that the proposed circuit breaker is to be placed in a electric power system where energy is relatively scarce, this solution needs at least some modification to be applied in the system of this paper. To use a resistive voltage divider to measure the voltage of the system can be used to interpret whether or not a fault has occurred. But to do this in series with the load amounts to having a shunt resistor, which brings the same benefits, but also the same drawbacks. If however, the voltage divider was connected in parallel to the load as in Figure 4.2, it would create a current path that could manage the power dissipation with the non-measured resistor and be sensed with a referenced comparator on the other resistor. This comparator will then drive a gate driver, which will then control the IGBT.

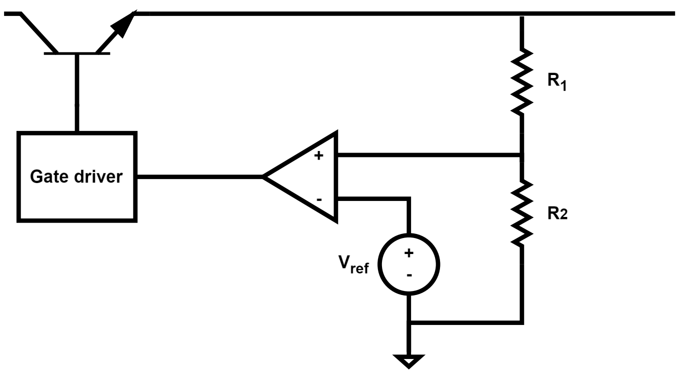

Figure 4.2: Fault detection using a shunt

4.4.1 Delay

The fault gets detected when the current reaches a certain threshold value. This threshold value was taken to be 600 A (1.2 times the nominal current) this is explained in section 5.4.1. From the moment the current passes the threshold there is a series of delays before the switch actually opens. Using the shunt resistor as fault detection mechanism the delays are within the comparator op-amp, the gate driver and the switch itself. From the data sheet it can be seen that the switch has a delay of $7.6\mu s$ [5]. Furthermore an op-amp has a slew rate of around 4V/μs [23] and 6V is required for the gate threshold voltage, therefore a delay of $1.5\mu s$ is required from the op-amp. Furthermore the gate driver has a delay 0f 0.037 μs [24], meaning that the total delay time in $9.137\mu s$, taking a 10% margin this gives a delay of 10 μs. This is an important factor that is taken into consideration during modeling as it can drastically effect the peak currents the circuit can reach.

4.5 Unidirectional to bidirectional

Throughout the report the main focus for simulation and testing will be based on the unidirectional circuit breaker. To adapt the unidirectional circuit breaker to a bidirectional circuit breaker an extra switch and snubber circuit is placed in series. The bidirectional circuit breaker is shown in figure 4.3. This extra switch is placed in opposite direction of the previous switch such that current flowing in the other direction can pass. Lastly in order to make the breaker bidirectional a diode should be placed in parallel with the switches allowing current opposing the switch to flow through the diode. A double snubber circuit is required as the second switch is also required to be protected against the voltage drop [7].

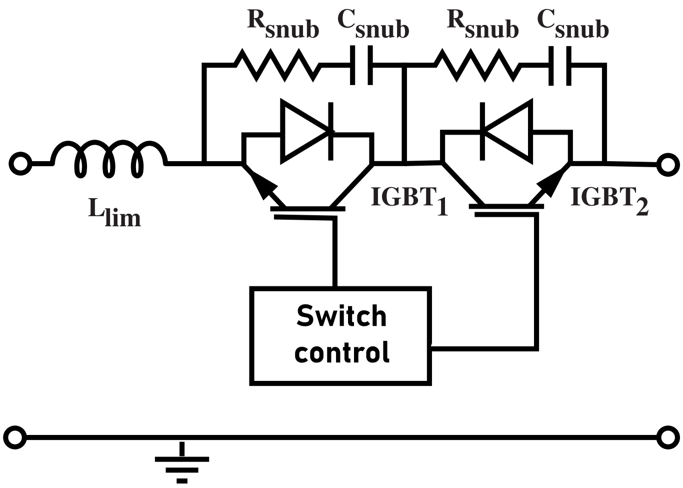

Figure 4.3: The final circuit breaker design of a unidirection circuit breaker with current limiter and snubber circuit

Chapter 5

Simulation

Knowing the different elements and the topology of the circuit breaker in question, it is most useful to determine the influence of the components and operation conditions on the behaviour of the circuit breaker as a whole. To achieve this, a model is built in Matlab's Simulink environment to simulate the circuit breaker. This model is shown in figure 5.1. This model is the complete model with current limiting inductor and snubber circuit. Throughout this chapter the model will be simulated using a combination of different RLC components. The model is simulated with a voltage source of 3kV and a load of 6Ω such that the current is 500A. Furthermore the line impedance is $3 \cdot 10^{-3} + 2 \cdot 10^{-5} j\omega$ and the source impedance is $1 \cdot 10^{-3} + 1 \cdot 10^{-5} j\omega$. The different components of the model will be discussed in this chapter. The method to find the exact RLC values is described in Chapter 7.

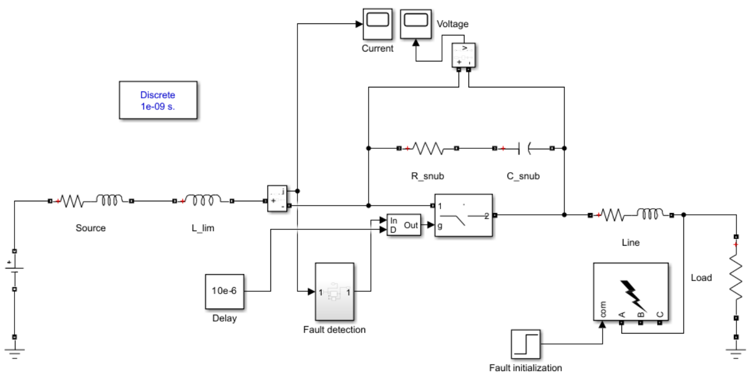

Figure 5.1: The simulation setup in simulink, used to simulate the full-scaled circuit breaker

5.1 IGBT

The IGBT in this topology serves as a solid-state switch to interrupt the power flow from the source to the fault. Of all components in the circuit breaker, the IGBT plays the most central role. However, using only the IGBT to break the circuit leads to some problems. As the fault cannot be detected instantly, the current rises unimpeded until some delay has passed. Interrupting this high current suddenly creates a voltage surge across the IGBT. This leads to voltage and current peaks far beyond the nominal operating range, as can be seen in Figure 1.4 from the introduction.

5.2 Inductor

To limit the current rise through the circuit, an inductor is used. This inductor ensures that the current does not exceed component ratings between the fault occurrence and interruption of the switch. Choosing a high inductance would seem to solve this easily, but this slows down the system under nominal operation and causes an even higher voltage peak over the switch. Figure 5.2 shows that indeed the current overshoot is kept within 1500 A, but with a slower response to start nominal operation. Also, Figure 5.2a still has an even higher peak than the use of a switch alone, which can be seen in Figure 1.4a. On the other hand choosing a lower inductance may not be able to limit the current enough to keep the switch from breaking.

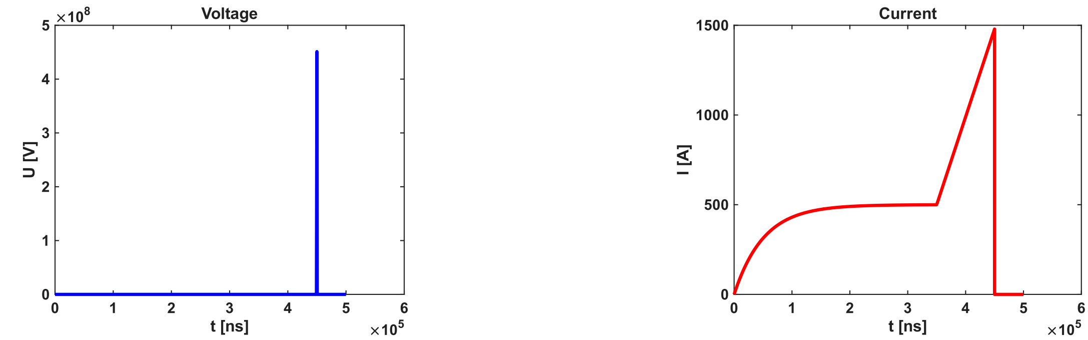

(a) Voltage behaviour of a switch with an inductor as circuit breaker

(b) Current behaviour of a switch with an inductor as circuit breaker

Figure 5.2: Voltage and current behaviour of a switch with an inductor as circuit breaker

5.3 Capacitor

To address the sudden rise in voltage, a capacitor can be used. This is because capacitors are known to be effective to smooth out sudden changes in voltage behaviour. However, using a capacitor in combination with an inductor can lead to oscillation. In Figure 5.3 it can be found that although the peak voltage and current stay within manageable boundaries, a heavy oscillation occurs that creates a negative current far below the nominal operation point that could be harmful to the circuit breaker and other adjacent systems. Choosing different capacitance values mainly changes the frequency of the oscillation and the peak value of the voltage and current.

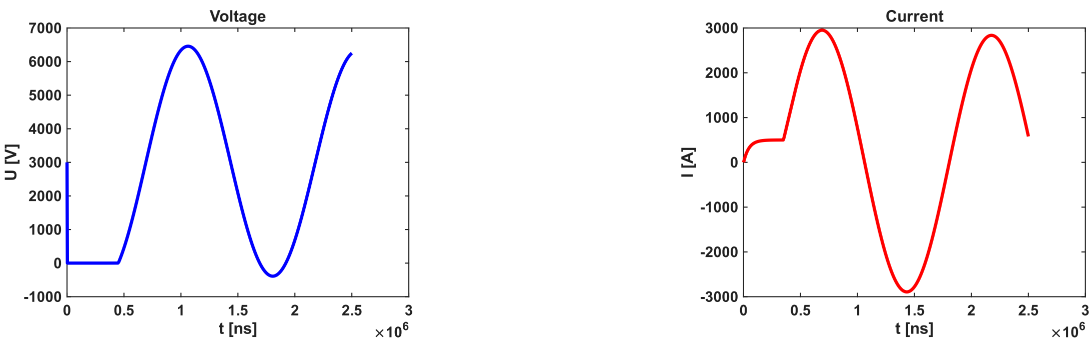

(a) Voltage behaviour of a switch, an inductor and a capacitor as circuit breaker

(b) Current behaviour detail of a switch, an inductor and a capacitor as circuit breaker

Figure 5.3: Voltage and current behaviour of a switch, an inductor and a capacitor as circuit breaker

5.4 RC-snubber

Combining the former methods to limit current overshoot and suppress voltage overshoot, a series branch of a resistor and a capacitor is placed in parallel with the switch, a so called RC-snubber, and an inductor is placed in series. The addition of this resistor prevents heavy oscillation while keeping the functionality of the inductor and capacitor.

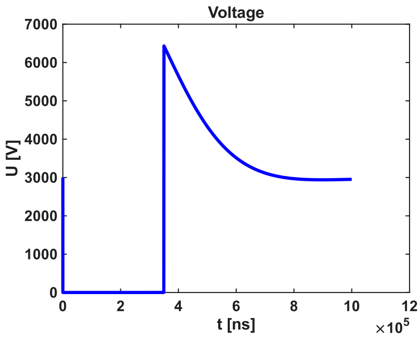

(a) Voltage behaviour of a switch, an inductor and a RC-snubber as circuit breaker

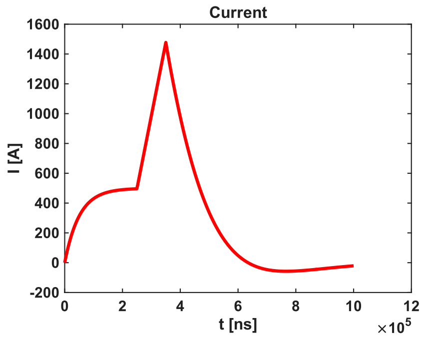

(b) Current behaviour detail of a switch, an inductor and a RC-snubber as circuit breaker

Figure 5.4: Voltage and current behaviour of a switch, an inductor and a RC-snubber as circuit breaker

5.4.1 Simulated fault detection

Another factor that determines the size of both voltage and current overshoot is the time that passes between fault occurrence and closing of the switch. If the circuit breaker starts to close the switch as soon as the fault occurs, this time is solely determined by internal propagation delays. This, however requires a perfect system where it is possible to instantly detect a fault. In reality, the system should have a lesser sensitivity to prevent the system from closing the circuit breaker in situations where the system parameters vary due to changes in the load. Also, like any sensing system, noise might seem like it behaves like a small fault event, even though the system is operating nominally. To prevent these false positives, the fault detection should monitor whether the system operates beneath a certain threshold. This means that when a fault occurs, is uninterrupted until it causes a disturbance beyond such threshold. To simulate this delay (from when the fault occurs to when it is detected) a fault detection block was added to the simulation. This fault detection block is connected to the current sensor and sends a signal to the switch when the current succeeds a threshold of 600A which is a factor of 1.2 times the nominal current. Using this method the fault detection system mentioned in section 4.4 is simulated. There is also a delay block added to the signal sent to the IGBT which takes into account the extra delay after the fault is detected which is calculated in section 4.4.1 to be 10μs

Chapter 6

Weight Equations

In this chapter a method to calculate the weight of the inductor and capacitor based on their inductance and capacitance is derived. These weight equations are required for the optimization which is explained in chapter 7. The optimization will eventually give the lightest combination of components for the circuit breaker. To calculate the lightest combination of components the mass of the components need to be derived which will be explained in this chapter. Solely the mass of the inductor and capacitor are considered as the mass of the resistor is negligible compared to the other components.

6.1 Capacitor

The mass of the capacitor was derived based on the fact that placing capacitors in series will increase their rated voltage, but decrease their capacitance, while placing them in parallel will increase their capacitance. A commercial capacitor with specified mass, capacitance, rated voltage and surge current was selected and used as a base value which could be adapted to fit the required capacitance. This commercial capacitor is a capacitor from TDK (more specifically B25620B1706K981). The ratings of the capacitor can be found in table 6.1. [25] contains a list of around 1000 different capacitors from TDK with different voltage ratings, weights and capacitance's including the capacitor chosen as the base value in this paper. This database will also be used to later compare the actual capacitance weight of the final capacitor with the calculated weight. The weight formula for the capacitor can be seen in equation 6.1. It considers the peak voltage of the system and capacitance required.

Table 6.1: The ratings of the capacitor chosen to derive the base values

	Rating
Capacitance	$70\,\mu F$
Mass	0.58 kg
Rated voltage	2000 V DC

$$m_C = m_0 \cdot \left(\frac{V}{V_0}\right)^2 \cdot \frac{C}{C_0} \tag{6.1}$$

Here m_C is the mass of a capacitor with capacitance 'C', 'm_0' is the mass of the base capacitor, 'V' is the peak voltage of the system if a capacitor with capacitance 'C' is placed in the system, V_0 is the rated voltage of the base capacitor, 'C' is the capacitance of the desired capacitor for in the system and 'C_0' is the capacitance of the base capacitor.

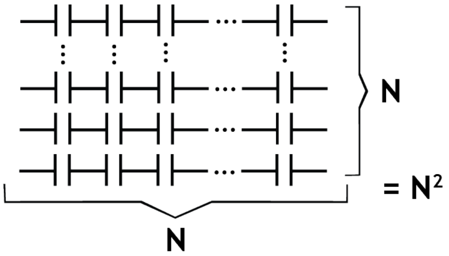

Figure 6.1: This figure shows the increase in number of capacitors 'N' when required to placing capacitors in series to deal with higher system voltages.

Placing capacitors in series to reduce the voltage over a capacitor, requires the capacitors to also be placed in parallel to maintain the capacitance value. If a larger peak voltage is required than the base voltage more capacitors need to be placed in series. However this means that the capacitance decreases meaning that the number of capacitors placed in series need to also be placed in parallel branches. This phenomenon is shown in figure 6.1. It demonstrates why the ratio V/V_0 is squared. Furthermore if the capacitance required is larger than the base capacitance more capacitors are required in parallel therefore the factor C/C_0 is considered. If for example a capacitor of 80 μF is required C/C_0 equals 2 meaning two capacitors in parallel are required.

6.2 Inductor

An inductor is typically made by winding a conductor around a core to create a magnetic circuit that can transduce electrical energy in a magnetic field. The choice of materials and geometry of both core and conductor influences the inductance and ratings of the inductor. In this paper, three types of inductor geometries are considered. These are the square core, toroid and solenoid inductors. As for the core materials, ferrite, iron, permendur (iron and cobalt alloy) and air are considered. Some properties of these core materials are found in Table 6.2.

Table 6.2: The (magnetic) properties of the different materials used for the core of the inductor

Material	**Relative permeability**	**Saturation point (T)**	**Density** (kg/m^2)
Iron [26][27][28]	200,000	1.6	7860
Ferrite [29][30]	2500	0.3	4900
Permendur [31][32]	800	2.1	8150
Air	1	∞	1.225

It is also important to consider the size of the cable that will conduct the current. The cable is made of copper which has a density of $8920\,\mathrm{kg/m^2}$ [33]. Considering the current density is $3\,\mathrm{A/mm^2}$ [34] and that the inductor should be capable of handling a nominal current of 500 A, a surface area of $167{\cdot}10^{-4}\,\mathrm{m^2}$ for the wire was calculated. This means the diameter of the wire is 0.0146 m. This diameter of the wire is the same for each inductor as it is solely dependent on the nominal current flowing through it, which is constant in all cases. The nominal current was chosen because that will be the current flowing through the cable most of the time, and when there is more current due to a fault event, this will only exceed the nominal current for at most 1 ms. Since this is such a short time, it is assumed in this paper that the thermal dissipation will be high enough in the wire to handle this peak without melting or causing damage to the system.

6.2.1 Square core

The design of the square core can be seen in Figure 6.2. The red box marked by the red dotted lines is where the wires will be wound around the core. To illustrate how the wire is wound around the core one turn is shown by the red line. The cross-section is the area marked 'A' in Figure 6.2. As the core is a square loop, the width of the core w_{core} is taken to be $\sqrt{A_{core}}$. The airgap is the size marked 'g' in Figure 6.2. Care is taken to evaluate the airgap length, as the equations used assume no fringing or losses in the airgap and a uniformly distributed magnetic field, resulting in the same magnetic flux density in the gap as in the rest of the core. The area of the window in the square is calculated based on how much space is required for the wire to go N turns through the inductor. This is dependent on the cross-sectional area of the wire, the number of turns it makes around the core and the fill factor. The fill factor is how much of the core is occupied by free space as circular wires cannot be perfectly placed next to each other. The area of the window is calculated using Equation 6.5. As the window is taken to be a square, the width of the window (denoted w_{window} in Figure 6.2) is then calculated by $w_{window} = \sqrt{A_{window}}$.

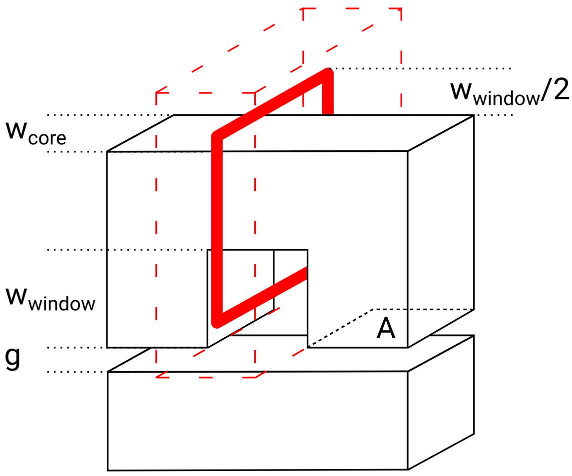

Figure 6.2: The square core inductor of which the weight equation is derived

Firstly, we relate the inductance to the magnetic flux density via the flux linkage:

$$\begin{aligned} \lambda &= N\phi \\ LI &= NBA \\ A &= \frac{LI}{BN} \end{aligned}$$

This gives:

$$A_{core} = \frac{LI}{BN} \tag{6.2}$$

Here, A_{core} is the area of the cross-section of the core measured in m^2 denoted with 'A' in Figure 6.2, L is the required inductance of the inductor measured in Henry, I is the peak current flowing through the wire denoted by the red line in Figure 6.2 measured in Ampère, B is the maximum magnetic flux density of the core material in Tesla and N is the number of turns the wire makes around the core.

Using Ampere's circuital law, an equation for the magnetic flux densities in the inductor is found:

$$\begin{aligned}
H &= \frac{I_{total}}{l_{total}} \\
I_{total} &= H l_{total} \\
NI &= H_{core} l_{core} + H_{gap} l_{gap} \\
NI &= \frac{B_{core}}{\mu_0 \mu_r} l_{core} + \frac{B_{gap}}{\mu_0} l_{gap}
\end{aligned}$$

And as can be seen in Table 6.2, $\mu_r >> \mu_0$. Combining this with the assumption that $B = B_{core} = B_{gap}$ we find:

$$\begin{aligned}
NI &= \frac{B_{core}}{\mu_0 \mu_r} l_{core} + \frac{B_{gap}}{\mu_0} l_{gap} \\
B &= \frac{NI}{\frac{l_{core}}{\mu_0 \mu_r} + \frac{l_{gap}}{\mu_0}} \approx \frac{NI}{\frac{g}{\mu_0}} \\
B &\approx \frac{\mu_0 NI}{g}
\end{aligned}$$

This gives the magnetic flux density as:

$$B = \frac{\mu_0 NI}{g} \tag{6.3}$$

To find 'g', this result is combined with the flux linkage of Equation 6.2 to find:

$$g = \frac{\mu_0 \cdot A_{core} \cdot N^2}{L} \tag{6.4}$$

Here, g is the width of the gap in meters, μ_0 is the permeability of free space as this approximates the permeability in the airgap, N is the number of turns and L is the inductance of the required inductor measured in henry. In the figure the airgap size is divided by two as Equation 6.4 calculates the total airgap, but in this case there are two airgaps so each should be half the size.

$$A_{window} = \frac{A_{wire} \cdot N}{\text{fill}} \tag{6.5}$$

Here, A_{window} is the area of the window in the square core measured in m^2, A_{wire} is the area of the cross-section of the wire in m^2, N is the number of turns and 'fill' is the fill factor of the wires.

Using these dimensions the volume of the core can be calculated using equation 6.2. The equation multiplies the area of the cross-section of the core 'A_{core}' with the length of the core. The length of the core is denoted by: $4 \cdot (w_{window} + w_{core})$, which can be derived from Figure 6.2. The mass of the core is now easily derived as the volume multiplied by the density.

$$V_{core} = 4 \cdot (w_{window} + w_{core}) \cdot A_{core} \tag{6.6}$$

Here, 'V_{core}' denotes the volume of the core in m^3, w_{window}, w_{core} and A_{core} are all denoted in figure 6.2 and measured in meters.

The area of the cross-section of the wire is already derived, however the length of the wire needs to be considered as well. The length of the wire is the number of turns multiplied by the length of one turn. This can be seen in Equation 6.7. Figure 6.2 demonstrates how the wire winds around the core. The length of one turn as shown in figure 6.2 was deduced to be $4 \cdot (w_{window} + w_{core})$. The total mass is then derived using equation 6.8.

$$l_{wire} = N \cdot 4 \cdot (w_{window} + w_{core}) \tag{6.7}$$

Here l_{wire} is the length of the wire, w_{window} and w_{core} are both shown in Figure 6.2 and measured in meters.

$$m_{total} = V_{core} \cdot \rho_{core} + A_{wire} \cdot l_{wire} \cdot \rho_{copper} \tag{6.8}$$

In this equation m_{total} is the total mass of the inductor in kg, V_{core} is the volume of the core as calculated in 6.6, A_{wire} is the area of the cross-section of the wire in meters, l_{wire} is the length of the wire in meters and ρ_{core} and ρ_{copper} are the densities of the core material and wire material respectively in $\mathrm{kg/m^3}$.

6.2.2 Toroid

For the toroid the calculations are similar to the square core inductor. The toroid core can be seen in Figure 6.3. The red circles show the turns of the wire around the core. The area of the cross-section of the core gets calculated as in Equation 6.2. The toroid is a square ring so the width of the toroid, denoted as '$\mathrm{w_{toroid}}$' in Figure 6.3 is equal to $\sqrt{A_{core}}$. The area of the gap in the core marked by 'g' in Figure 6.3 is calculated by Equation 6.4.

The inner radius of the toroid core marked r_{inner} in figure 6.3 is calculated using equation 6.9. It considers that the circumference of the inner circle needs to be large enough such that all turns of the copper wire can be placed next to each other. Therefore the diameter of the wire plus an isolation thickness of 1 mm at each side needs to be taken into account. This gives the circumference of the inner circle of which the radius can be deduced. The equation also adds r_{wire} as it otherwise considers the radius to the middle of the cable instead of the edge of to the core.

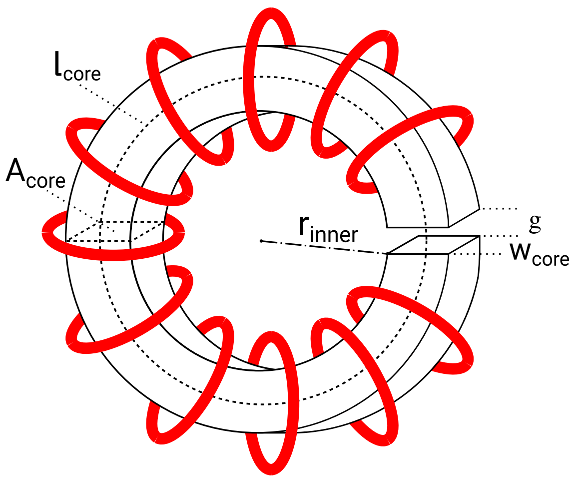

Figure 6.3: The toroid core inductor of which the weight equation is derived

$$r_{inner} = \frac{N \cdot (d_{wire} + 0.002)}{2 \cdot \pi} + r_{wire} \tag{6.9}$$

This equation gives r_{inner} as the inner radius of the toroid in meters. N is the number of turns, d_{wire} is the diameter of the wire and r_{wire} is the radius of the wire both in meters.

Using r_{inner} and w_{toroid} the length '$\mathrm{l_{core}}$' in Figure 6.3 can be derived. This can be seen in Equation

6.10. Using this length and the core area and density, the mass of the core can be derived.

$$l_{core} = \pi \cdot (r_i \cdot 2 + \frac{w_{toroid}}{2}) - g \tag{6.10}$$

Here, l_{core} is the length of the toroid in meters as indicated in Figure 6.3, r_{inner} is the inner radius of the toroid and w_{toroid} is the width of the toroid both in meters as indicated in figure 6.3 and g is the width of the airgap also in meters.

The mass of the wire is again the length of the wire multiplied by its cross-sectional area and density. The length of the wire is the perimeter around the core which is four times the width as the cross-section of the core is a square. This can be seen in equation 6.11. The total mass of this coil is then calculated using equation 6.12.

$$l_{wire} = 4 \cdot w_{toroid} \cdot N \tag{6.11}$$

$$m_{total} = l_{wire} \cdot A_{wire} \cdot \rho_{wire} + l_{core} \cdot A_{core} \cdot \rho_{core} \tag{6.12}$$

6.2.3 Solenoid

For the solenoid only an air core is considered. This means that there is no saturation point to take into consideration. The solenoid can be seen in Figure 6.4. The diameter of the solenoid was considered to be 0.25 m. The reason this was considered as diameter is such that the height of the coil does not become too large for use in an aircraft. Using this diameter the area of the coil becomes $\pi\frac{d^2}{4}$ which is $0.0625\,\mathrm{m}^2$. The number of turns required for the solenoid was then calculated using Equation 6.15 which is derived from Equation 6.13 which considers the inductance required and Equation 6.14 which considers the length of the solenoid.

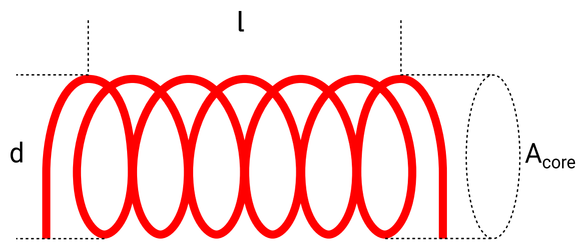

Figure 6.4: The toroid coil of which the weight equation is derived

$$L = \frac{\mu_0 N^2 A_{solenoid}}{l} \tag{6.13}$$

Here, L is the required inductance in henry, μ_0 is the permittivity of free space which is approximated by $4\pi \cdot 10^{-7}$, N is the number of turns, $A_{solenoid}$ is the cross-sectional area of the solenoid in m^2 and l is the length of the solenoid in meters [35].

$$l = N(d_{wire} + 0.002) \tag{6.14}$$

Here 'l' is the length of the solenoid in meters, and N is the number of turns. The factor 0.002 is considered as isolation between each turn which also adds to the length of the coil. This spacing is required such that the current density in the wire can remain at $3\,\mathrm{A/mm^2}$ as winding the turns closer together will lead to higher temperatures and thus lower current density.

The number of turns can then be derived from Equations 6.13 and 6.14:

$$N = \frac{(d_{wire} + 0.002) \cdot L}{\mu_0 A_{solenoid}} \tag{6.15}$$

Now that the number of required turns is deduced the total length of the wire can be calculated using Equation 6.16. This equation accounts for the fact that each turn has a length of $\pi \cdot d$, which is the circumference of the solenoid.

$$l_{wire} = \pi \cdot d \cdot N \tag{6.16}$$

Here, l_{wire} is the length of the wire in meters, 'd' is the diameter of the solenoid as denoted in Figure 6.4 in meters and N is the number of turns.

Knowing the length, cross-sectional area and density of the wire the mass can be calculated using Equation 6.17

$$m_{total} = A_{wire} l_{wire} \rho \tag{6.17}$$

where A_{wire} is the area of the cross section of the wire and l_{wire} is the length of the wire calculated using $\pi d_{wire} N$ and ρ_{copper} is the density in this case of copper.

A weight equation for all the three types of inductors is now derived. A function was created including these equations which takes as input the inductance required, number of turns and peak current and can output either the smallest weight or the weight of each inductor. This code can be seen in appendix A.3

6.2.4 Comparison of different inductor

To analyse the effect of the core geometry, type of material and number of turns on the weight of the inductor, a comparison between the different inductors was made. Firstly the core geometry was compared. In Figure 6.5a the mass of the cores based on different inductance values was calculated and plotted. It can be seen that in all cases the toroid is the lightest therefore most suitable in this application. Interesting to note is that the mass of the solenoid seems to go up in a staircase fashion. This is because a 'ceiling' function was used when determining the number of turns required for the inductor. Furthermore the mass of the inductor is also dependent on the number of turns of the wire around the core. This dependency can be seen in figure 6.5b. As the mass of both cores are dependent on the number of turns, the number of turns will be taken into consideration in the optimization. It is also interesting to note that the mass of the toroid is less susceptible to the number of turns than the square core. This can be derived from the mass equations provided above.

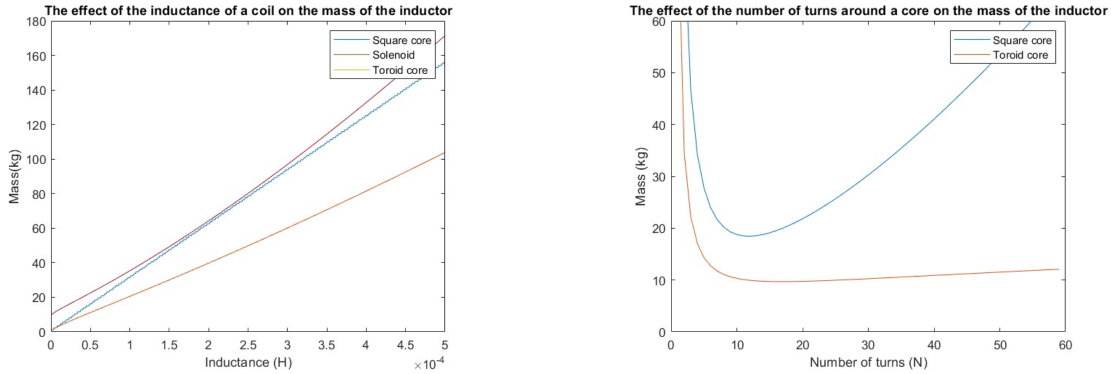

(a) A graph showing how the inductance effects the mass of the inductor for different core geometries. Considering a peak current of 1500 A and 18 turns

(b) A graph showing how the number of turns effects the mass of the inductor. Considering a peak current of 1500 A and inductance of 42 μH

Figure 6.5: The effect of inductance and number of turns on the mass of the inductor based on different core geometries

Using different materials with different densities and saturation points affects the mass of the final inductor based on the required inductance. Ferrite is a material with a relatively low saturation point of 0.3 T. Even though it does have a lower density, the area required for the core still needs to be a lot larger than for the other materials due to the low saturation point. The lower density does not compensate for lower saturation point as it is the heaviest inductor. Permendur has the highest density, however it also has the highest saturation point. Due to the high saturation point the core cross-section area can be reduced so much that it compensates for the larger density of the material. An overview of the properties of the different materials can be seen in table 6.2.

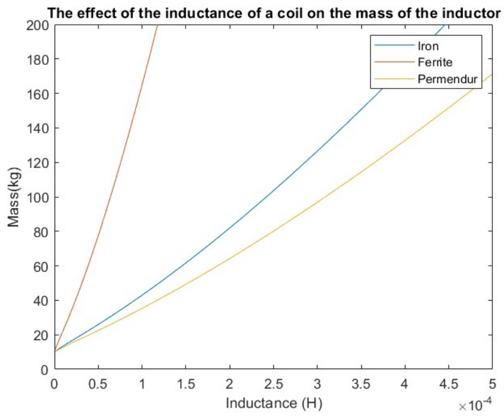

Figure 6.6: Effect of change in the required inductance on the mass of a square core considering different material. The peak current was set to 1500 A and the number of turns is 18.

Chapter 7

Optimisation

The system as of yet is dependent on several variables. Setting these variables determines the way the circuit breaker functions. There are 4 main variables to tune chosen in this paper, the inductance of the current limiter, the capacitance, the resistance of the RC-snubber circuit and as explained in Chapter 6 the amount of turns plays a big role in the total weight.
These values should be chosen in a way that creates the optimal balance in the system, since a higher inductance would limit the current rise even more, this would also cause a higher peak in voltage which needs to be suppressed by the RC values. The balancing of these values can be done in different ways, two of these are discussed in the chapter.

First of all the system should always keep the peak-voltage and peak-current under a set threshold. These thresholds are based on what can be seen in Chapter 2.
Secondly since the circuit breaker is made for aviational use the main thing to consider is the weight.
The weight is the actual property that needs to be minimal while still respecting the ratings of the system.

Regarding the inductance and capacitance, the lower the values the higher the peaks. The resistance however suppresses the voltage peak more the lower the value gets. With a lower resistance the resistor should still be able to handle the high power and heat that gets generated during the fault. The lower the resistance the more difficult this becomes.

Lastly the amount of turns in the inductor determines a lot for the weight, finding the optimum for this can make drastic changes for the final weight.
To find the optimum of this 4-variable problem an optimisation is required since a local minimum can probably be found using trial and error, but a global minimum is very difficult to find without trying almost all values. This optimisation can be done using MatLab. Here there are 2 ways to do it in MatLab explained and compared.

7.1 Brute Force

This first and easiest method is using a brute force script. All that is needed is a lower bound, an upper bound and a step size for every variable. The workings of the brute force is visualized in Figure 7.1

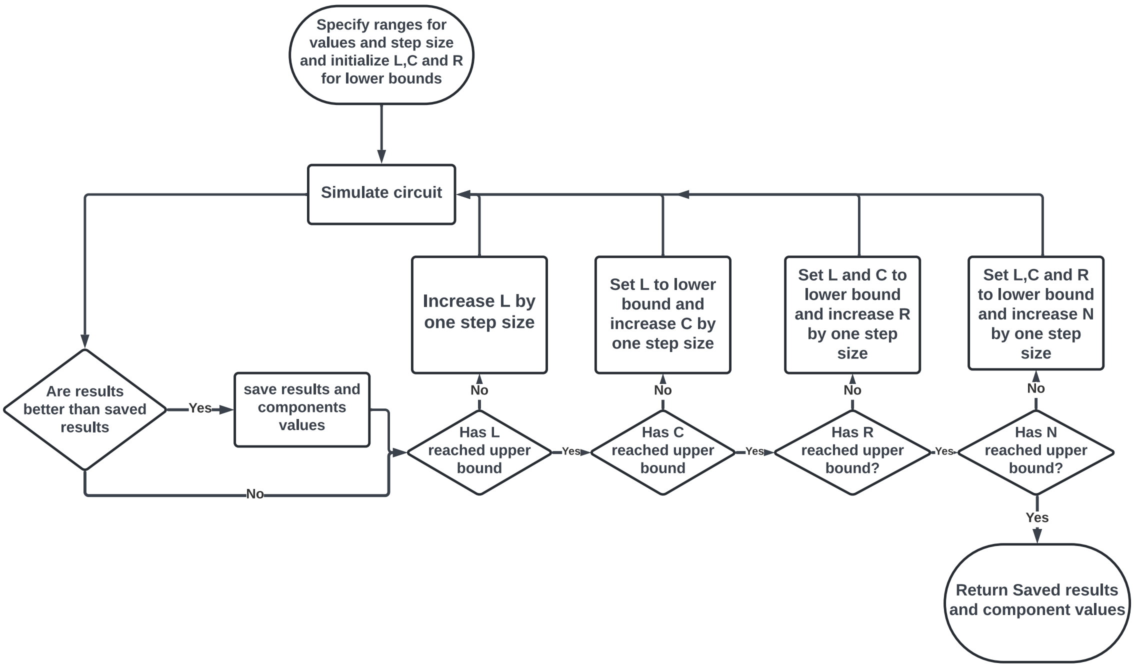

Figure 7.1: A visualisation of a brute force algorithm for determining L, R, C and N

The brute force script runs a simulation using the lower bound values for R, C, L and N, collects the data and increase one variable with its step size, when it has cycled through all values for this variable it will increase the next one by one time its step size and repeat the process. This causes the script to run a simulation for every possible value and collect the data. By making the program return the option where the peaks were under a certain threshold but still minimize the weight, using the equations explained in Chapter 6, the design can be optimised.
This method has a few downsides however, first of all it is incredibly slow. Since it has to run a simulation for every option it can drastically increase the time with bigger ranges of values. If only 100 values are tested for every variable it already needs to run a 100 million times, assuming 1.5 seconds per simulation this will take 4.75 years. This is clearly not a reasonable option at all.
The second thing is that this program works on discrete values for the variables. It is unknown at first in what range the values should be and thus the chance exists that a wrongly chosen step size could skip the global minimum.

7.2 Genetic Algorithm

The second way to make an optimisation is using a more efficient algorithm. The optimisation algorithm used in this paper is the genetic algorithm. The workings of the genetic algorithm are visualized in the flow chart shown in Figure 7.2.

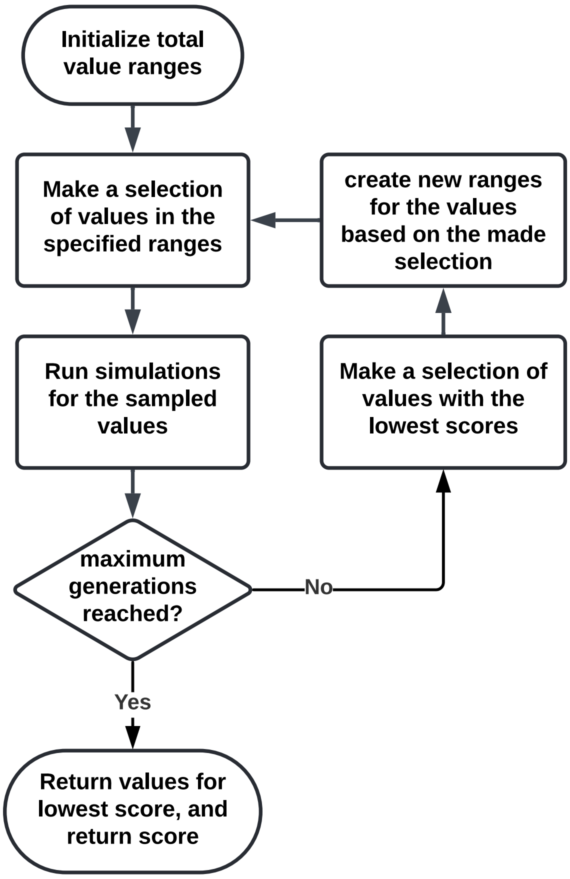

Figure 7.2: A visualisation of a genetic algorithm for determining L, C and R

The genetic algorithm is based on biological genetics and natural selection, by running different generations and letting the individuals with the lowest scores reproduce into the next generation. This should result in a generation of all lower scores. At the final generation the lowest score should be the global minimum.

For the implementation in the circuit breaker a score needs to be set for each simulation. Based on this the generations are determined. Since the weight needs to be minimized, the program should calculate the weight of each component and add them, resulting in the score. The formula to calculate the weight is derived in Chapter 6. Since the weight of the resistor is almost negligible compared to the weight of the capacitor and inductor, it is not included in the calculated score.

The genetic algorithm works by setting upper and lower limits for the inductance, capacitance, resistance and the number of turns. The algorithm chooses random values spread along these ranges, and runs the simulation and stores the results. The amount of values it simulates is specified in the script as the population size. After the full population size is simulated, it takes a couple of individuals with the lowest score and picks new values around these individuals for the next round of simulation. This way the algorithm slowly zooms in on a global minimum.

The reasoning behind using this algorithm is that it becomes very good at escaping local minima. Other algorithms involving just one solution, like for example simulated annealling, might get stuck on a good solution and keep evolving on those values, even though this could be a local minima instead of the global minimum. With genetic algorithm it keeps a population of contenders, meaning it will easily escape a local minima and that is perfect in the case of this implementation.

The final version of the code can be seen in A.4. An overview of the parameters are given in 7.1.

Parameter	**Value**
Population Size	200
Max Generations	30
Lower Bounds	Inductance: $1 \cdot 10^{-6}$ Resistance: 1 Capacitance: $1 \cdot 10^{-6}$ Amount of turns: 1
Upper Bounds	Inductance: $1 \cdot 10^{-3}$ Resistance: 50 Capacitance: $1 \cdot 10^{-3}$ Amount of turns: 100
Time Taken (Minutes)	87

Table 7.1: Genetic Algorithm Parameters

Chapter 8

Final Design

The final circuit breaker design can be seen in Figure 4.3. It is a design that consists of a current limiting inductor to limit the fault current and an RC snubber to limit the overvoltage. The values for the inductor, resistor and capacitor were deduced using the optimization algorithm discussed in Chapter 7. These values can be seen in table 8.1. The final design using the derived values was simulated in Simulink. The voltage over and current through the switch were recorded and plotted as can be seen in Figure 8.1. The voltage reaches 3.6 kV and the current reaches a peak magnitude of 1020 A. This is within the specifications mentioned in Chapter 2. Furthermore the peak current lasts 350 μs, which is also within specifications.

Table 8.1: The values for the final design of the circuit breaker

Component	**Value**
Inductor	42 μH
Capacitor	40 μF
Resistor	3 Ω

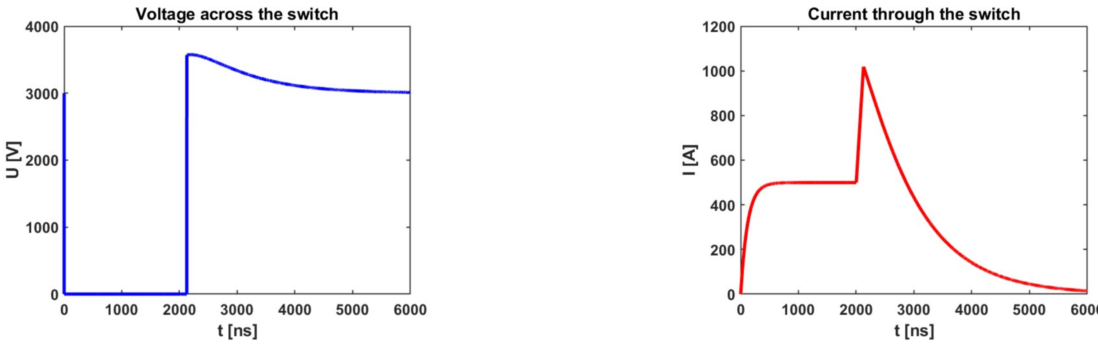

(a) Voltage across the breaker when a fault occurs at 0.2ms

(b) Current through the breaker when a fault occurs at 0.2ms

Figure 8.1: Voltage and current behaviour of the final breaker design simulated in simulink

8.1 Component selection

In order to further find the weight and determine the reliability of this design it is important to distinguish the different components that need to be used as they need to have the correct value, but also correct current and voltage ratings for the nominal operating conditions and short circuit conditions.

8.1.1 Capacitor

A capacitor that falls within the needed voltage and current ratings and has the required value of 40 μF is a power film capacitor from TDK (more specifically B25620C1706K981*) [25]. The choice opted towards power film capacitors as these are often used for providing protection for devices subjected to high voltage spikes, which is exactly the use for this capacitor in the breaker [36]. As can be seen in the data sheet this capacitor has a maximum surge current of 4.5kA, voltage of 2kV and capacitance of 40 μF. Placing two in series and then two in parallel will increase the voltage rating to 4kV and keep the capacitance at 40 μF, which falls within the ratings required for the circuit breaker snubber. The four capacitors combination weights 1.92kg. This weight is comparable to the weight derived from the weight equation which states that the mass is 1.96kg. It is important to note, especially for the reliability analysis later on that the dielectric of the capacitor is made of polyurethane which is a type of plastic often used for high voltage applications as it can better handle the higher voltages [36].

8.1.2 Resistor

The resistor value is low, which is difficult to realise for high power systems, as the resistor needs to have enough insulation to deal with the high currents and voltages, which often increases the resistance, which in this case is required to be kept low. The resistor in the snubber circuit needs to be able to dissipate the energy from the current flowing through it when the switch is open until zero current. Furthermore it should be able to withstand a voltage peak of 3.6kV. The current through and voltage over the snubber resistor was measured in the simulation and the energy dissipated by the resistor was calculated using equation 8.1 [37]. The energy dissipated over the resistor was 350J. A resistor was found which has a fusing energy of 632J and resistance of 4.7Ω [38]. Placing two of them in parallel provides 2.35Ω, which is close to the required value. The volume of both resistors in parallel is $2.972 \cdot 10^{-6}$ m^3, multiplying this by the density of the ceramic material (6000 kg/m^2 [39]) used for the resistor gives a mass of 17.8 grams was calculated. The resistor used is a wire wound resistor which are common resistors used in high power and high surge current application.

$$E = \int_{t_0}^{t_0+\Delta t} V \cdot I \, dx \tag{8.1}$$

where E is the energy dissipated in joules, V is the voltage in volts, I the current in Ampere and t the time in seconds [37]. t_0 is the time at which the switch opens and Δt is a next point in time after the peak current.

8.1.3 Inductor

The optimisation returns the set of values with the lowest weight. For the final design the optimisation returned 42 μH with a peak current of 1020 A, in Table 8.2 the weights for different materials and types of inductors are shown.

Table 8.2: Masses of different types of inductors with various materials. The air core inductor does not use these materials and has a single mass value.

	Iron (kg)	**Ferrite (kg)**	**Permendur (kg)**
Square Inductor Mass	19.2521	46.1197	17.3169
Toroidal Inductor Mass	9.39806	30.7934	7.6561
Solenoid Inductor Mass	13.9015 (Air)		

The inductor with the lowest weight is the toroidal inductor made from permendur. If this were to be designed the dimensions can also be extracted from the MatLab script. These dimensions are shown in 8.3

Table 8.3: Dimensions of the Toroidal Inductor

Dimension	Value (cm)
Inner Radius of Core	5.47
outer Radius of Core	8.84
Width of the Air Gap	1.10
Width of the Core	3.37

8.2 The total system

In table 8.4 a summary of all the components and their mass can be found. The mass of the switch is taken from the data sheet of the switch shown in appendix A.1. The total mass of the system is around 10kg, which is under the specifications mentioned in Chapter 2. It is however important to note that the weight of this circuit breaker is for a nominal current of 500 A and nominal voltage of 3.6 kV. Higher nominal conditions could lead to a heavier breaker.

Table 8.4: The mass of each component for the upscaled circuit breaker

Component	Mass (kg)
Thin film capacitor	1.92
Wire wound resistor	0.0178
Permendur toroid core inductor	7.6
Solid state switch	1.4
Total mass	11

Chapter 9

Testing

In order to support the decisions made based on the simulation, a version of the simulated breaker was built and tested using scaled down ratings. The test setup can be seen in Figure 9.1. The gate drivers that control the fault switch and the switch in the circuit breaker are both controlled by an Arduino microcontroller where the signals that control t_{delay} are controlled within microseconds.

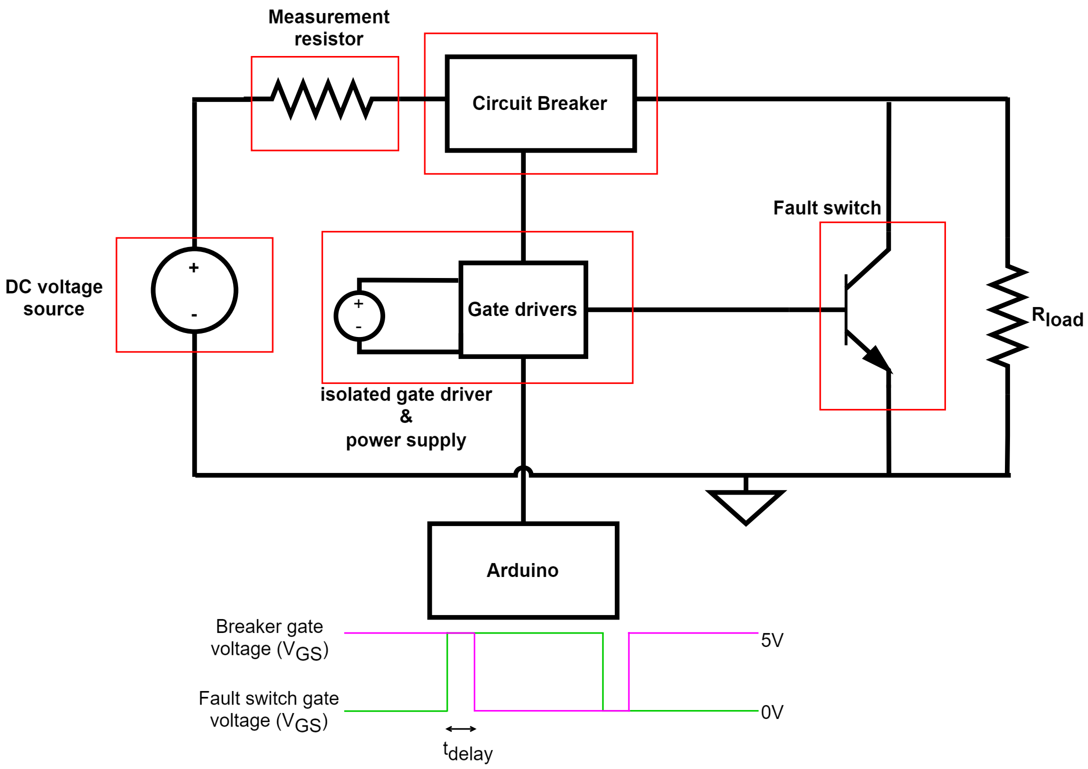

Figure 9.1: The general setup used for testing

9.1 Test Set-up

The point of having a general layout of the test setup is that this makes it possible to keep everything consistent and only change the circuit breaker block and analyse its behaviour. The components besides the circuit breaker itself are explained below.

9.1.1 Gate Driver

The gate driver circuit was assembled during this research and was developed by Weichuan Zhao in the High Voltage Lab at the Delft University of Technology. In the setup two MOSFETs are used that need to be opened and closed at different times. To open the gate, the gate to source terminal voltage needs to exceed the internal threshold voltage of the MOSFET. Since the source terminals of both MOSFETs are in the current path of our test circuit and exhibit transient voltage behaviour, the voltage required to open the gate varies. To be able to instead drive the MOSFETs from a constant control signal, two gate driver circuits are used. These drive the voltage on the MOSFET terminals from an auxiliary power source based on the timing of the signal from the Arduino microcontroller.
To verify the function of the gate drivers, they were measured at the output. These gate drivers decouple the input electrically from the output at the MOSFETs with a DC/DC converter. However, sufficiently powerful pulses from the test circuit were still measured when testing the system in operation

9.1.2 Arduino

Testing the delay, as described in Subsection 4.4.1, is fundamental for testing the behaviour of the breaker. This delay is implemented as the difference between the opening of the fault switch and the closing of the breaker switch. In an ideal case the current in the prototype should be measured and the breaker should close after reaching a certain threshold, but due to limited resources the delay is put in manually using an Arduino Uno R3 board. The Arduino code can be found in A.2. The effect of using this delay will be further explained later in this chapter.

9.1.3 Current measurement

To know the behaviour of the system correctly a fundamental aspect is the current through the system. To measure this there are different methods available all with their own benefits and downsides. Both methods will be explained below.

Measurement resistor

As shown in Figure 9.1 a measurement resistor is used in the final test setup. Since the current through a resistor is always equal to the voltage across it divided by its resistance, it is possible to know the current through the resistor, and with that through the circuit breaker, by measuring the voltage and dividing it by its resistance.
A big problem with using a resistor here is the internal inductance of the resistor. When the resistor has an inductance that is too high, it will create peaks in the voltage, leading to incorrect current estimation. Too negate this a nickel wire is used. Nickel wire has a relatively high resistance, meaning it is possible to use only a small piece of wire as resistor, which has little inductance, and still handle the currents. After measuring the resistance of the wire it was set at 0.33, meaning any voltage measured across it could be multiplied by 3 to obtain the current. The inductance was measured at 300 nH. Apart from the small added inductance the resistor naturally also adds resistance to the entire circuit, thus limiting the current and creating power loss.

Current measuring probe

Another way of measuring the current is setting up a current measuring probe. The probe works by measuring the magnetic field around a wire and dependent on how strong the field is outputs the current. This can be directly read onto the oscilloscope. This method is a lot more accurate than the previously mentioned measuring resistor, but also requires more equipment.

These methods are very different and as mentioned the resistor is easier but less accurate, while the current probe is expensive and requires more equipment. In Figure 9.2 the current measurement using a probe is compared to the current measurement using a resistor. It can be seen that both measurements are similar, however that the current probe measures a slightly higher current. The figure shows the behaviour of the current through the system when the fault occurs with an applied input voltage of 10V. Due to the internal resistance of the circuit being 1 Ω the maximum current that can be measured is 10A.

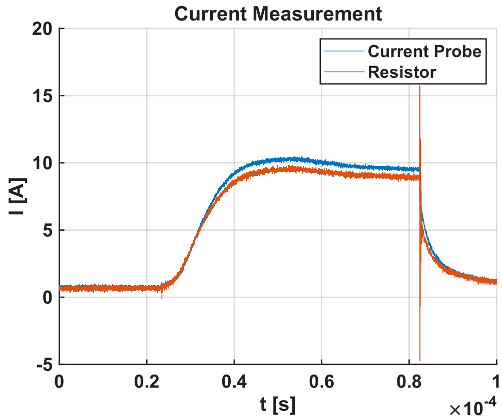

Figure 9.2: The current measured using the voltage over a resistor compared to the current measured using the probe

9.2 Test plan

To test the circuit, probes are put into place to measure different voltages and current. The source-drain voltage of the breaker switch is always measured to make sure this does not exceed the rated limit of the MOSFET. The voltage delivered by the source is decreased and increased to receive different results and see how everything scales. During testing, Arduino code will be used as shown in Appendix A.2. In this chapter it is important to note that the delay can not be done using a threshold due to lack of resources. Instead a delay was programmed into the code of the Arduino.

9.2.1 Tested delay

In the tests the Arduino will control the full delay as explained in Section 9.1.2. In reality a lower inductor causes the current to reach the threshold faster, this also means that in the small delay time after the threshold is reached the current reaches higher values. By using a set delay in the Arduino code the speed of increase is not considered, meaning that for very high inductance value the total delay from fault to interrupt is the same, in reality the time until threshold was reached would be smaller when the inductance gets smaller.

9.2.2 Tested Circuits

The tested circuits were all measured at 4 Volts delivered by the source. The order of tested circuits follow the same pattern as the simulation. First the circuit breaker part as shown in Figure 9.1 is implemented as only a switch. Since it is known and verified using simulation that using only a switch as breaker will create high current and voltage peaks, the switch is chosen with rating much higher than the nominal operation ratings. This means that even under the high stress of the peaks the switch will not break and will be able to deliver results to confirm the simulations.
After knowing that everything works and confirming the simulations the next step becomes adding a current limiter. The value for this inductor is found using the optimisation script explained in Subsection 7.2. After confirming that the results still match the expected result, so a lower current slope and higher peak voltage, the last element can be added.
This is the RC-Snubber, These values are also derived from the optimisation algorithm. After this the tested circuit breaker should meet the same requirements as mentioned in the Chapter 2, but scaled to the new ratings.

9.3 Down scaling

Up until now the Simulink model and genetic algorithm have been used for finding values for the full-scaled circuit breaker. To use the model to find component values for the down-scaled breaker a few adaptations to both the model and the algorithm needs to be made. Firstly in the model the voltage source is now set to 4V instead of 3kV and the load is set to 10 Ω as this was the load connected to the circuit during testing. The total source impedance was set to $0.3 + j\omega 2.5 \cdot 10^{-5}\Omega$ and the line impedance was set to $0.7 + j\omega 1.5 \cdot 10^{-5}\Omega$. From calibration tests it was evident that the internal resistance of the system was 1Ω. Then by comparing the results of the test to the results of the simulation the internal inductance was set to the given values. Lastly the fault detection mechanism threshold was set tot 1.2 times the new nominal current which was $0.4 \cdot 1.2 = 4.8A$.

In the optimization algorithm the threshold values were adapted to deal with the new current and voltage over the system. The threshold voltage was set to 1.2 times the nominal voltage. The threshold current was set to 3 times the nominal current and the peak negative current was set to -0.5 times the nominal current. Now that the optimization algorithm and simulink model were set for the downscaled model the values for the downscaled RLC were found and are as follows: 1.9 Ω, 51 μH and 17.8μF.

9.4 Results

9.4.1 Interference

In these results shown below it is important to note that everything was measured using probes and wires. Since the switch opening creates an enormous voltage spike it also creates an electric field, this results in interference on every measured channel. A difference can be seen when measuring the input and output of the gate driver. Inside the gate driver are resistors designed to stop the fast fluctuations and slow down the MOSFETs. This difference can be seen in Figure 9.3. It can be seen that the spike in voltage together with the following fluctuations measured at the output of the gate driver is a lot smaller than at the input of the gate driver which is due to the resistors placed in the gate driver circuit.

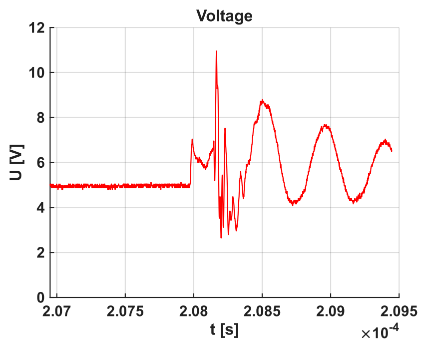

(a) The signal measured at the input of the gate drivers

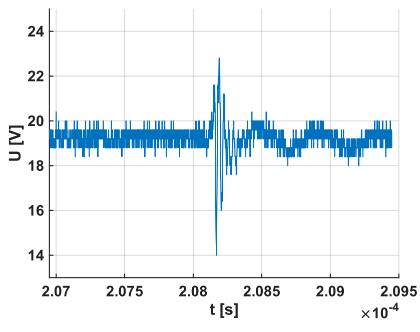

(b) The signal measured at the output of the gate drivers

Figure 9.3: The difference between measuring at the input and output of the gate drivers

9.4.2 No protection

The first part of the testing is shown in Figure 9.4 and consists only of the MOSFET as the circuit breaker.

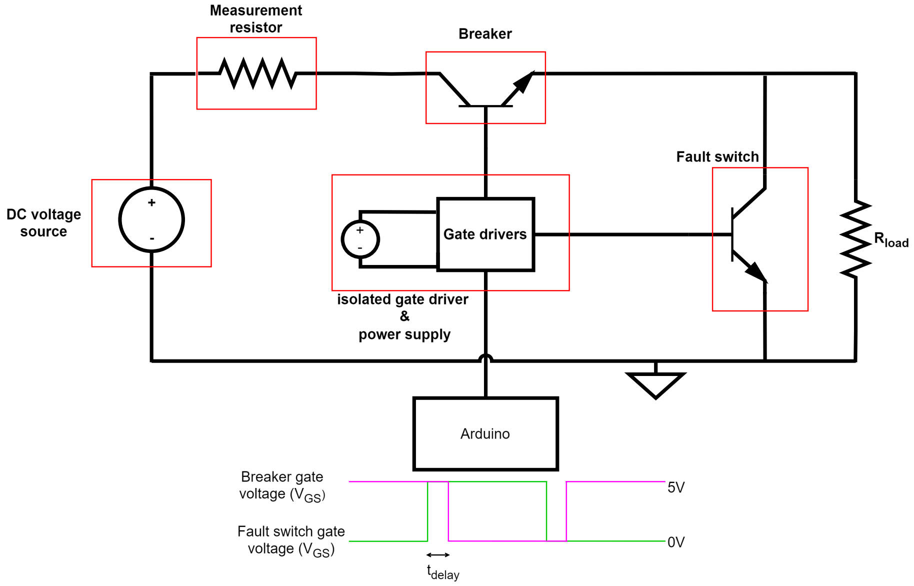

Figure 9.4: The test setup using only a switch as Breaker

The MOSFET used with high enough ratings to withstand the expected high peaks is STF34N65M5. The most important results measured are the source to drain across the breaker switch and the current through the switch. It is expected that a high peak is created for both of these values, a lot higher than the input ratings. In an up scaled implementation it is not possible to create switches that can handle these rating-peaks so this is the exact reason why extra protection is necessary.

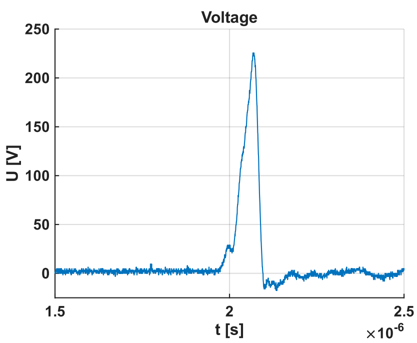

(a) Voltage across switch with no extra protection

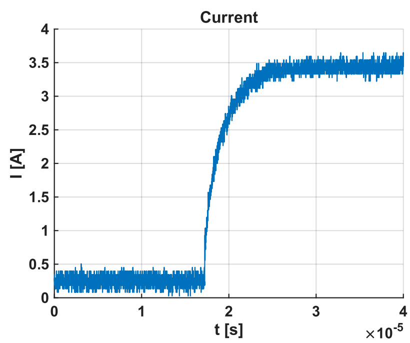

(b) Current through switch with no extra protection

Figure 9.5: Voltage and current behaviour of the tested circuit with no protection

It can be seen from Figure 9.5a that the voltages reaches a peak of 225 V and from figure 9.5b that the current quickly saturates towards 4A. Ideally the current should rise slowly such that the switch can open before the current saturates. Reducing the rate at which current rises is done using the current limiting inductor. In these tests the delay of the breaker was set to $60\mu s$ such that the complete saturation of the current can be analysed. It is further important to note that when measuring the voltage the oscilloscope was zoomed in to the breaker closing time, while for measuring the current the oscilloscope was zoomed in to the time at which the fault happens. This is also the case for the other plots in this chapter.

9.4.3 Current limiter

The next step is controlling the current peak shown in 9.5b. To do this a current limiter, in the form of an inductor, is added in front of the switch. The new set-up can be seen in Figure 9.6.

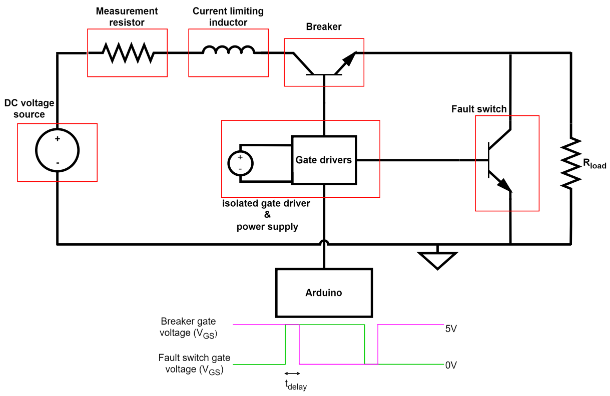

Figure 9.6: Test set-up with current limiter

The inductor added is made using wire wound around a toroid core three times. Measuring the inductor results in a value of 55 μH which is close to the value obtained from the optimisation, but not perfect. Even though the inductor value is not the optimal value it still proves the workings of the current limiter.
With this test the difference between reality and test becomes very apparent from the delay difference as described in Section 9.2.

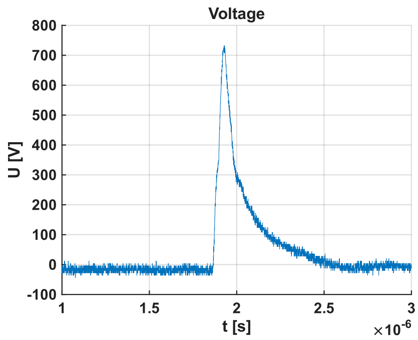

(a) Voltage across switch with current limiter

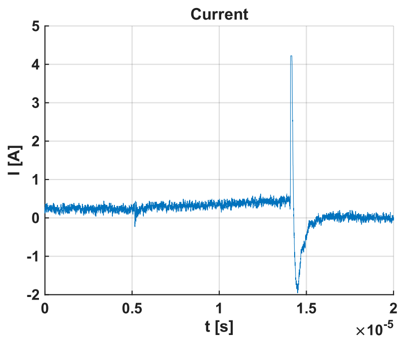

(b) Current through switch with current limiter at 10 μs delay

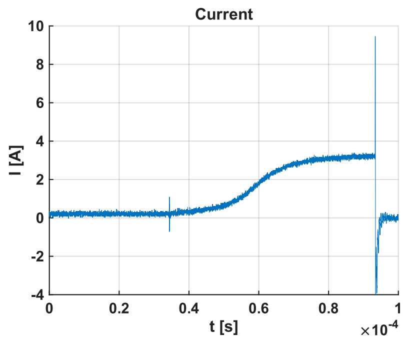

(c) Current through switch with current limiter at 60 μs delay

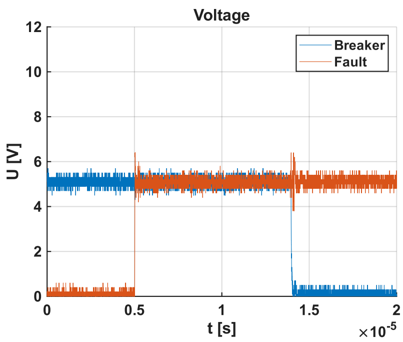

(d) Voltage signals controlling the breaker (blue) and short circuit (red) at 10 μs delay

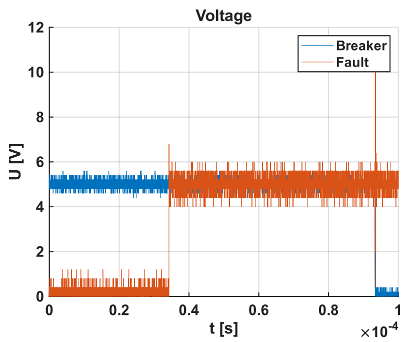

(e) Voltage signals controlling the breaker (blue) and short circuit (red) at 60 μs delay

Figure 9.7: Voltage and current behaviour of the tested circuit with current limiter

In Figure 9.7 the results clearly show that the inductor does what it is put in place for, limiting the current. The rise in current from zero until saturation now takes 30μs instead of the initial 10 μs without inductor. The testing was done once with a delay of 10 μs to see how high the current is when it gets cut off and once with a delay of 60 μs to see how long it takes for the current to saturate. This can be seen in figure 9.7b and 9.7c respectively. It can be seen that without inductor the current is already saturated once the breaker opens, while with inductor the current is not even at 1A. The problem as also explained in Chapter 5 is that the voltage peaks even higher, now even reaching to the limits of the used MOSFET. The voltage peak is now at 710V as can be seen in figure 9.7a instead of 225V which was the case without the inductor. This creates the reason for the next stage of the circuit breaker.

9.4.4 RC-Snubber

The only problem with the circuit as it is, is the high voltage peak. This could destroy the switch or even create arcing across components. As explained in Chapter 4, the circuit needs an RC-Snubber circuit to suppress the voltage peak. The resulting test setup can be seen in Figure 9.8.

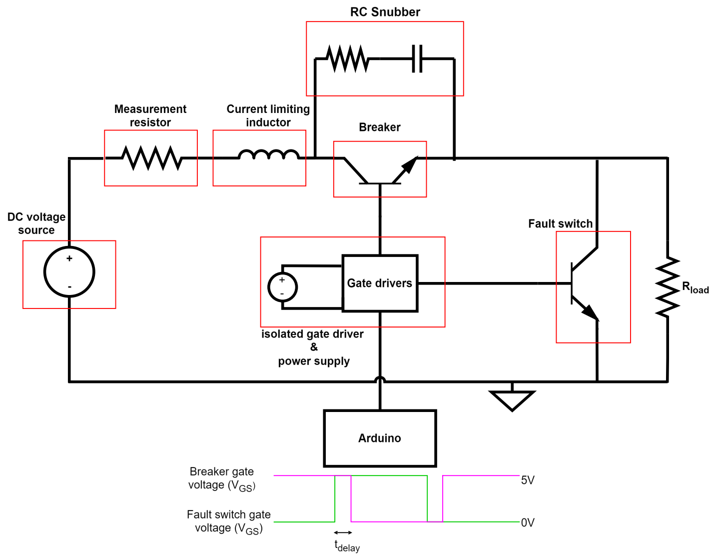

Figure 9.8: Test Setup for the full circuit breaker

To get the correct value for the capacitor, 3 capacitors were placed in parallel, two of $\sim 6.8\mu F$ and one of $\sim 4.7\mu F$, the resulting capacitor was measured at 17.8 μF. For the resistor, 3 resistors of $\sim 5.4\Omega$ were placed in parallel resulting in a resistor of 1.9 Ω. The results of the total circuit are shown in Figure 9.9.

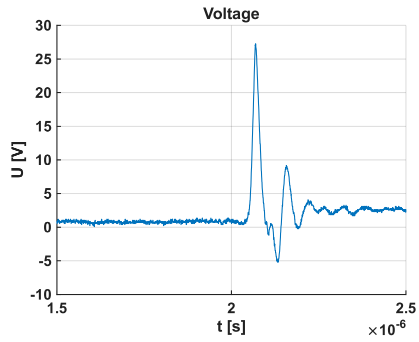

(a) Voltage across switch with current limiter and RC-snubber

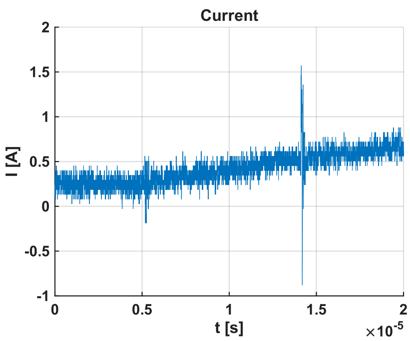

(b) Current through switch with current limiter and RC-snubber at 10 μs delay

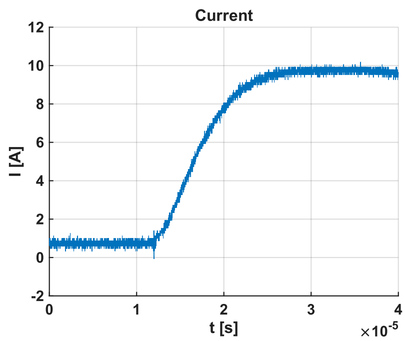

(c) Current through switch with current limiter and RC-snubber at 60 μs delay

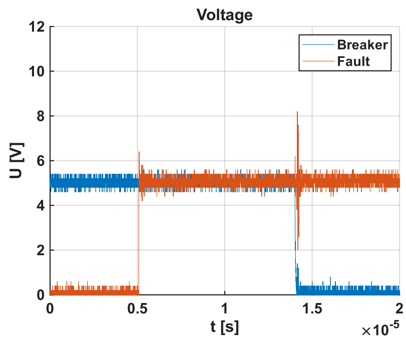

(d) Voltage signals controlling the breaker (blue) and short circuit (red) at 10 μs delay

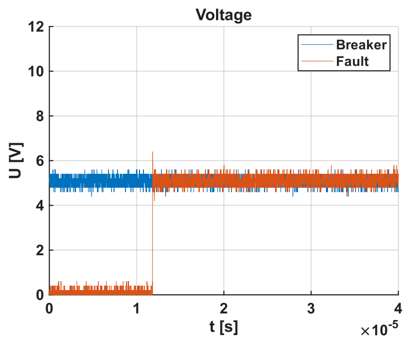

(e) Voltage signals controlling the breaker (blue) and short circuit (red) at 60 μs delay

Figure 9.9: Voltage and current behaviour of the tested circuit with current limiter and RC-snubber

From figure 9.9a it can be seen that the voltage peak is now a lot smaller (26V instead of 710V), which is due to the snubber circuit. As the voltage is now limited due to the snubber the input voltage was also increased to 10V, making it such that in figure 9.9e the current reaches 10A.

The figure below shows the entire set-up of the test circuit including the full breaker. The large capacitor attached in parallel to the power source of the system is used to provide more current to the system in one test.

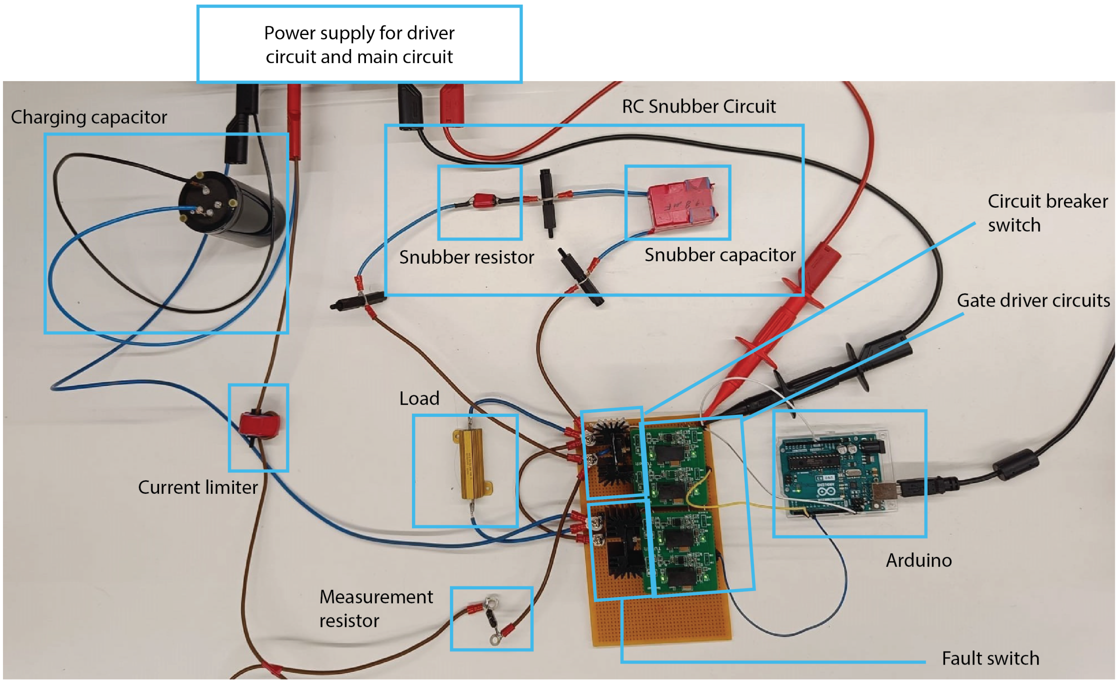

Figure 9.10: The general setup used for testing

Chapter 10

Reliability of the circuit breaker

Knowing the failure rate of the circuit breaker is an important concept when considering the reliability of a system. The failure rate will be calculated in this chapter based on a fault tree analysis. As demonstrated throughout the testing and simulations if any of the protective elements (the inductor, capacitor or resistor) breaks, the circuit breaker will fail due to unsatisfactory suppression of overcurrent and overvoltage. Furthermore if the switch breaks the circuit breaker will fail as well. Either the switch creates a short such that the load cannot disconnect in case of a fault or the switch becomes open such that no current can flow to the load in nominal operating conditions. In this analysis only the switch failure considering the short is taken into account as this is a fatal failure and an open circuit is not.

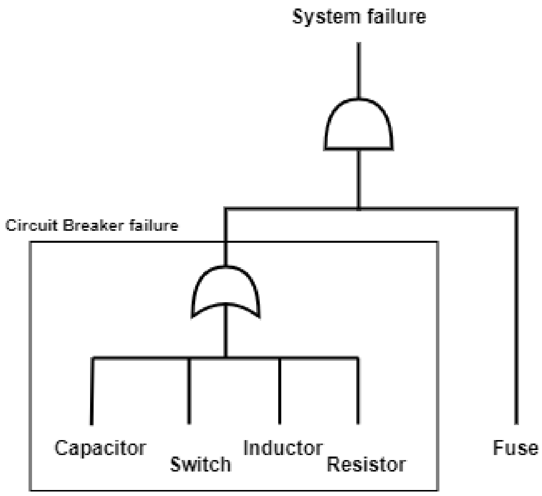

Figure 10.1: FTA of the breaker

In Figure 10.1 an FTA can be seen. The idea of an FTA is to visualise the fault probabilities in a system and show how it would propogate through the system. The benefit of using an FTA instead of something like an RBD (Reliability Block Diagram), is that the FTA is very easy and clear when it comes to simpler systems like the system shown above. It can easily be seen what subsystems are connected and how a fault propogates.
If any of the components of the breaker fails it would cause a breaker failure. In the diagram these are connected through an OR-Gate, meaning if either the capacitor fails OR the switch OR the inductor OR the resistor it will cause a failure. Apart from the breaker there is also a fuse in the system. A fuse can be placed in series with a circuit breaker as a last resort. The fuse and breaker are connected through an AND-Gate, meaning both the breaker AND the fuse need to fail for the fault to propagate further. In this

chapter the influence of the fuse on the reliability of the system will also be further discussed.

Now that the fault tree is produced the failure rates of the components need to be determined. These failure rates will be mostly calculated based on formulas found in [40]. Each component has a certain base failure rate. However there are different factors that can influence this failure rate. These factors include the quality of the component and the environment in which the component is used.

Especially the environmental factor is important as the breaker is used in an aircraft which has differing environmental conditions than on the ground. Furthermore the reliability is also based on the range of the value of the component (e.g Ω, kΩ, μF. etc). The general formula can be seen in equation 10.1. All components are considered to operate at an ambient temperature of $40°C$ as this is the operating temperature of most circuit breakers [41]. The breaker is further design to have a maximum operating temperature of $85°C$. This is mainly because the maximum operating temperatures of components such as the capacitor fall within this range. This temperature will be maintained using a cooling system.

$$\lambda_p = \lambda_b \pi_Q \pi_E \pi_v \tag{10.1}$$

Whereby λ_p is the failure rate of the component given in Failure/10^6 Hours, λ_b is the base failure rate, π_Q is the quality factor, π_E is the environmental factor and π_v is the value range. The quality factor is based on what the application is of the component. A component made for use in space travel for example has a higher reliability than a component made for use in the industry. The components that are considered in this paper have quality indicator P, which stands for industrial and production. A list of all quality indicators can be found in appendix A.5. The environmental indicator is A_{IC} which is 'airborne inhabited cargo'.

10.1 Reliability of the capacitor

The reliability for specifically a fixed plastic film capacitor was calculated using [40]. Both the ambient temperature 'T_A'and stress 'S' of the component influences the base failure rate of this component. The maximum rated temperature of the resistor is $85°C$, however the operating temperature, T_A is $40°C$. The stress factor is the ratio of the operating voltage and rated voltage which for this capacitor is 3.6 kV/4 kV so 0.9. Plugging these values into Equation 10.2 the base failure rate was calculated to be 0.037. Furthermore the coefficient π_v was calculated with $1.3C^{0.077}$ whereby C is the capacitance. Further coefficients were taken from a given table in [40]. A summary of all coefficients can be found in table 10.1. Multiplying them together gives a failure rate of 0.0262 Failures/10^6 Hours.

$$\lambda_b = 0.0005[\frac{S}{0.4}^5 + 1]e^{2.5(\frac{T+273}{358})^{18}} \tag{10.2}$$

Table 10.1: The values used to deduce the failure rate of the capacitor

Coeffieient	Values
λ_b	0.037
π_v	0.596
π_Q	0.3
π_E	4
λ_p	0.0262

10.2 Reliability of the resistor

For the resistor the reliability was calculated using a similar approach. The resistor that is considered is a fixed wire wound resistor. The base failure rate is again based on the ambient temperature and the stress factor. The stress factor in this case being the rated energy it can dissipate and the calculated energy which is 350/632=0.55. λ_b is using Equation 10.3 calculated to be 0.0157. The other coefficients were found in the tables provided in [40]. A summary of all coefficients can be found in table 10.2. The total failure rate is 0.01889 Failures/10^6 Hours.

$$\lambda_b = 0.00148 e^{(\frac{T+273}{298})^2} e^{(\frac{S}{0.5})(\frac{T+273}{273})} \tag{10.3}$$

Table 10.2: The values used to deduce the failure rate of the resistor

Coeffieient	Values
λ_b	0.0157
π_v	1
π_Q	0.3
π_E	4
λ_p	0.01889

10.3 Reliability of the inductor

Again the inductor failure rate is calculated in a similar way to the capacitor and resistor failure rate. In this case the base failure rate only takes into account the hot spot temperature and the maximum operating temperature. The inductor is designed in such a way that the hotspot temperature is at $85°C$ as this is the maximum rated temperature of the system. The maximum operating temperature of the inductor is $150°C$ as this is the maximum temperature copper can get [42]. Using equation 10.4 the base failure rate was calculated to be 0.00046. Furthermore in this case π_v is not dependent on the value of the inductor, solely on whether the inductor is fixed or variable, which in this case the inductor is fixed giving it a coefficient of 1. The other coefficients were found in the tables provided in [40]. A summary of all coefficients can be found in table 10.3. The total failure rate is 0.00069 Failures/10^6 Hours. The failure rate of the inductor is much lower than the rest as the core and wire are very robust. Furthermore the maximum temperature of the system is far below the maximum operating temperature of the copper.

$$\lambda_b = 0.000335 e^{(\frac{T_{HS}+273}{329})^{15.6}} \tag{10.4}$$

Table 10.3: The values used to deduce the failure rate of the inductor

Coeffieient	Values
λ_b	0.00046
π_v	1
π_Q	0.3
π_E	5
λ_p	0.00069

10.4 Reliability of the switch

Unike the components mentioned above the IGBT switch failure rate is not calculated using [40]. Figure 10.2 from [43] shows the failure rate of IGBTs over the years given in FIT (Failure/10^9 Hours). Extrapolating the plot to 2024 it can be deduced that nowadays the failure rate has decreased to around 2 FIT which is 0.002 Failures/10^6 Hours. This failure rate however only considers switches at ground level. Within an aircraft at high altitudes there is more presence of cosmic radiation which can further degrade the switch and effect its reliability. According to [44] equation 10.5 can be used to find the influence of the altitude difference on the failure rate. Considering a height of 5800 this factor is 38.48. This value seems high, but could be accurate as silicon is greatly effected by the increase in cosmic rays at higher altitudes. The total failure rate of the IGBT is given by the base failure rate of 0.002 multiplied by the height factor of 38.48 giving a failure rate of 0.0796 Failures/10^6 Hours.

$$\pi_E = e^{\frac{1-(1-\frac{h}{44300})^{5.26}}{0.143}} \tag{10.5}$$

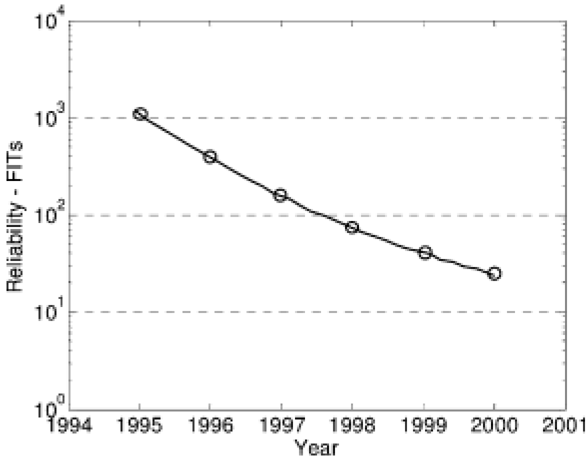

Figure 10.2: The FIT rate of an IGBT switch over the years [43]

10.5 The influence of fuses

A fuse failure can be categorised into four main categories namely: a primary, a secondary, tertiary and non-functional failure. A primary failure is when the fuse is not able to interrupt the current while keeping peak voltage and current values under required ratings. A secondary failure is when a fuse fails because it does not match its rated values due to production errors such as bad connections. A tertiary failure takes into account when a fuse surpasses its rated values but does not explode. The non-functional failure considers small losses due to for example rusting or cracks in the fuse. This failure category will however not be taken into consideration with the failure rate of the fuse as it does not lead to fuse failure [45].

According to [45] the failure rate of a fuse is 0.002 faults per year which translates to 0.228 Failures/10^6 Hours or $228 \cdot 10^{-9}$ Failures/hour. Shown in table A.5 are the failure rates of all components and the total failure rate of the system with and without a fuse.

Table 10.4: The failure rate of each component and the combined failure rate of the circuit breaker with a fuse

Component	Failure rate (Failures/Flight hour)
Thin film capacitor	$26.2 \cdot 10^{-9}$
Wire wound resistor	$18.9 \cdot 10^{-9}$
Permendur toroid core inductor	$0.69 \cdot 10^{-9}$
Solid state switch	$79.6 \cdot 10^{-9}$
Fuse	$228 \cdot 10^{-9}$
Total failure rate (without fuse)	$125.39 \cdot 10^{-9}$
Total failure rate (with fuse)	$285 \cdot 10^{-12}$

By adding a fuse in series to the circuit breaker it reduced the reliability by a factor of 438. This is because in the FTA the fuse and circuit breaker are connected via an 'OR' gate which indicates that their failure rates get multiplied, which reduces the failure rate unlike with the 'AND' gate where the failure rates are added up. A fuse is therefore certainly worth taking into consideration for in an aircraft. It should however be taken into account that a fuse is a one time use system.

Chapter 11

Conclusion & Discussion

11.1 Discussion

The results found in this paper mostly match the specifications described in Chapter 2. The breaker is able to handle the nominal currents and voltages. The peaks in both the current and voltage fall below the peak level indicated in the requirements. Furthermore the weight of the breaker is below the required weight. The results found in Chapter 9 discuss some unexpected behaviour that occurred when driving the MOSFETs, but this was manageable for the experiments that were conducted for this paper. Another unexpected result however, was more difficult to work around. This was the current saturation that occurred at lower levels than expected and stopped the rising of current sooner than the closing of the breaker. This might be due to a higher impedance of the circuit than was intended, but would require significant investigation to determine this or other causes. As for the results, the influence of the inductor on the rate this current rises was still observable, as well as the blocking of the current by the closing of the switch. Thus, these results were still considered valuable for this paper. The scope of this project was at first broadly defined. This creates possibilities as well as challenges. To use an optimisation algorithm for circuit design is a non trivial approach in a bachelor's study, but educational to explore. The weight equations used, and derived, came with logical results, even though it is hard to say whether the inductor equation is accurate. Furthermore, the application of practical skills, such as building and measuring power circuits was rather valuable as well. Some of the challenges that were faced include subsystems such as those of the gate drivers and fault detection. Designing and building such systems besides the rest of the circuit breaker was pressing given the time frame of this paper. This is why these were not thoroughly discussed. Also, having a broad scope makes the scrutiny under which choices are assessed uncertain. Although it can be expected of this that decisions need to be made on sound theory and research, the amount of detail was not always straightforward to gauge.

11.2 Conclusion

To design a DC circuit breaker for the electric power system for an all electric aircraft, multiple breaker topologies were considered. A unidirectional solid-state circuit breaker was found to be the most suitable due to the few necessary components leading to decreased weight and increased reliability, both desirable traits for aviational components. This topology requires the use of solid state switches and suppressors of both currents and voltages that would break said switches in the case of a short circuit fault. For the solid state switch an IGBT was chosen for its low power losses in the operation conditions of the power system. As for the suppressors, a passive inductance and RC-snubber were chosen for the current and voltage respectively. This due to both their simplicity and reliable operation in the case of repeated faults during operation. The IGBTs however need a controlling signal to operate them, therefore a fault detection system was derived to sense fault events and drive the IGBTs accordingly. The unidirectional circuit breaker was modeled to simulate what impact different component values have on the performance of the design. Furthermore weight formulas were derived for the different components in the circuit breaker, such that the lightest combination of components can be selected for the breaker. The results of the simulation model and the weight formulas were then used in a genetic algorithm to optimise component values to yield the best performance and lightest weight within system specification. These values were then assessed to see if such components are available and how much the circuit breaker would weigh in total including the switch. The component values that were found match those that are available on the market and the total weight of the main components (without fault detection system) of a unidirectional circuit breaker amount to 10.50 kg. To determine if the approach was viable for designing such a circuit breaker, a downscaled model was designed, built and tested. The results show that the components influence the behaviour of the circuit breaker in a similar way as the simulation show. The inductor slows the rise of current during a fault, but increases the voltage, and the RC-snubber limits the voltage, but adds oscillation, and combining both of these in this topology protects the switch when closing a short circuit fault. Lastly the reliability of the circuit breaker was calculated based on the failure rates of different components. The failure rate of the circuit breaker with a fuse was derived to be $285 \cdot 10^{-12}$ Failures/flight hours. The total summary of the breaker, the components, their weight and reliability can be found in appendix A.6.

A possible next step in researching this topic is building a prototype that is more resembling of the upscaled version. In this paper the testing was mostly done to prove the workings of a general circuit breaker, but not whether the weight will match the optimisation. The optimisation can be used to find the optimal weight for a downscaled and testable setup, and see how accurate the weight optimisation is by building it. If this is validated then a fully upscaled model can be made and tested with increasing ratings. This should handle the full scale so should withstand everything below it. After this is validated the circuit breaker should be pushed to its limits and the tests should be repeated many times to get an estimation of the reliability. This research was completely based on 3 kV and 500 A, this was chosen because this is the nominal rating in most parts of the aircraft. In certain places in the aircraft the ratings will even reach 4320 A, this would require a bigger circuit breaker of about 150 kg, this makes the AEA seem impossible again. Further research should also focus on the breakers with higher ratings and see if those can be made lightweight.

Appendices

Appendix A

Appendices

A.1 Final switch data sheet

FZ750R65KE3

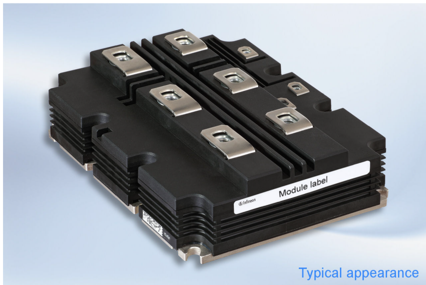

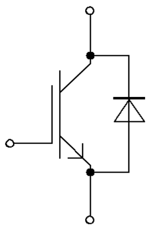

V_{CES} = 6500V
$I_{C\ nom}$ = 750A / I_{CRM} = 1500A

IGBT,Wechselrichter / IGBT,Inverter
Höchstzulässige Werte / Maximum Rated Values

Kollektor-Emitter-Sperrspannung Collector-emitter voltage	T_{vj} = 125°C T_{vj} = 25°C T_{vj} = -50°C	V_{CES}		6500 6500 5900		V
Dauergleichstrom Continuous DC forward current		I_F		750		A
Kollektor-Dauergleichstrom Continuous DC collector current	T_C = 80°C, $T_{vj\ max}$ = 150°C	$I_{C\ nom}$		750		A
Periodischer Kollektor-Spitzenstrom Repetitive peak collector current	t_P = 1 ms	I_{CRM}		1500		A
Gate-Emitter-Spitzenspannung Gate-emitter peak voltage		V_{GES}		+/-20		V
Abschaltverzögerungszeit, induktive Last Turn-off delay time, inductive load	I_C = 750 A, V_{CE} = 3600 V V_{GE} = ±15 V R_{Goff} = 6,8 Ω T_{vj} = 25°C T_{vj} = 125°C	$t_{d\ off}$		7,30 7,60		µs µs
Gate-Schwellenspannung Gate threshold voltage	I_C = 100 mA, V_{CE} = V_{GE}, T_{vj} = 25°C	V_{GEth}	5,40	6,00	6,60	V
Gewicht Weight		G		1400		g

A.2 Gate Driver Code

```
// delayMicroseconds() works reliably in the range of 3 microseconds
    and up to 16383

void setup() {
// // // _asm_("nop\n\t");
DDRD=B00010100;
noInterrupts()

PORTD=B00000100;
delayMicroseconds(100);
PORTD=B00010100;
delayMicroseconds(10);
PORTD=B00010000;
delayMicroseconds(100);
PORTD=B00000000;
delayMicroseconds(10);
PORTD = B0000100;
}

void loop() {}
```

Arduino code

A.3 Weight formula

```
%Function to find the mass of an inductor considering different cores
    and
%materials
%input number of turns, inductance required and peak current
%outputs the inductor with lowest mass

function [score]= mass_inductor(N,L,I)

%permeability of materials
mu_0=4*pi*10^(-7);
mu_r=[200000, 2500, 800]; %iron, ferrite (manganeze zinc), permendur

%saturation point
B=[1.6,0.3,2.1]; %iron, ferrite and permendur

%density
rho=[7860,4900,8150];%iron, ferrite, permendur
rho_copper= 8920;

%diameter of the copper wire
A_wire=(500/3)*10^(-6);
r_wire=sqrt(A_wire/pi);
d_wire= 2*r_wire;


%FOR SQUARE COIL
%fill factor of copper
fill = 0.4;%you cannot place cicles perfectly against eachother

%finding A and g
A_core=L.*I./(B.*N);
g=mu_0.*A_core.*N.^2/(2.*L);

%finding geometry of the core
w_core=sqrt(A_core);%width and depth of the core are the same
A_copper=A_wire.*N;
A_window=A_copper./fill;%area of the window needs to be large enough
    for the wires
w_window=sqrt(A_window);

%finding the mass
L_cable=(4*w_window+4.*w_core);%length of copper wire
mass_copper=L_cable*A_wire.*N.*rho_copper ;
mass_core=(A_core .* rho) .* (4 * w_core + 4 * w_window);
mass_total=mass_copper+mass_core;

%SOLENOID
d=0.25;
A_sollenoid=pi*(d/2)^2;%area of the solenoid
n=ceil(L*(r_wire*2+2e-3)/(mu_0*A_sollenoid));%number of turns to
    achieve required inductance
```

```
l_coil=n*(r_wire*2+2e-3);%length of the coil
l_cable=pi*d*n;

mass=A_wire*l_cable*8850;

%FOR TORROID
r_i=N*(d_wire+0.002)/(2*pi)+r_wire;%finding the inner radius based on
    width of wire
d_i=r_i*2;%diameter of inner circle
%alternative way of finding r_i based on copper fill
%A_window = A_copper/fill;
%r_i=realsqrt(A_window./pi)

A_toroid=L*I./(N.*B);%area of the torroid based on B=LI/NA
g=mu_0.*A_toroid.*N^2/L; %airgap based on saturation point
w_toroid=realsqrt(A_toroid);%radius of solely the toroid
r_o=r_i+w_toroid;%total radius from center
length=pi*(d_i+w_toroid/2)-g;%length of the torroid if unrolled

%mass of toroid
mass_copper=4.*w_toroid.*A_wire.*N.*rho_copper;
total_mass_torroid = A_toroid.*length.*rho+mass_copper;

%total mass of the system
%mass_total=["mass square", mass_total,"mass air core", mass, "mass
    torroid",total_mass_torroid]
mass_total=[mass_total, mass, total_mass_torroid];
score=min(mass_total);
end
```

Weight formula

A.4 Optimisation

```
% Define fitness model
function [score] = simple_fitness(params)
    % Formulas for the weight of each component should go here after
        derivation
    weightL = params(1);
    weightC = params(3);
    load_system('Switch_Fault_thresh');
    currentp= 3*500;
    voltagep= 1.2*3;
    valleyp= -0.5*500;

    % Set parameter values in the Simulink model
    set_param('Switch_Fault_thresh/L_lim', 'Inductance', num2str(
        params(1)));
    set_param('Switch_Fault_thresh/R_snub', 'Resistance', num2str(
        params(2)));
    set_param('Switch_Fault_thresh/C_snub', 'Capacitance', num2str(
        params(3)));
```

```matlab

    % Run the simulation
    simOut = sim('Switch_Fault_thresh');

    % Set valley_current as lowest current point to check if there is
        high oscillation
    valley_current = min(simOut.CurrentOut);

    % Set peak_current and peak_voltage
    peak_current = max(simOut.CurrentOut);
    peak_voltage = max(simOut.VoltageOut);

    % Initialize offset
    offset = 0;

    % Set rating boudaries for the system
    % When ratings are not met, the score should be very high so it
        will be
    % disregarded by algorithm
    if peak_current > currentp || peak_voltage > voltagep ||
        valley_current < valleyp
        offset = 100000;
    end

    % Close the Simulink model
    close_system('Switch_Fault_thresh', 0);

    % Calculate total score
    score = weightL + weightC + offset;
    %score = peak_current + peak_voltage;
end

% For reproducibility
rng default
FitnessFunction = @simple_fitness;
numberOfVariables = 3;

% Set upper and lower bounds for [Inductance, Resistance, Capacitance]
lb = [1e-6, 1, 1e-6];
ub = [1e-3, 50, 1e-3];

% Set a few extra algorithm options
options = optimoptions('ga', 'PopulationSize', 200, 'MaxGenerations',
    30, 'UseParallel', false, 'Display', 'iter');
[x, fval] = ga(FitnessFunction, numberOfVariables, [], [], [], [], lb,
    ub, [], options);

% Print score and parameters for lowest score
x,fval
```

OPtimization

A.5 Quality Designators for reliability analysis

Quality designator	Explanation
S	Space
R	High reliability
P	Industrial or Production
M	Military
Lower	Lower quality or commercial grade

Table A.1: The quality designators and what they stand for

A.6 Summary of final breaker values

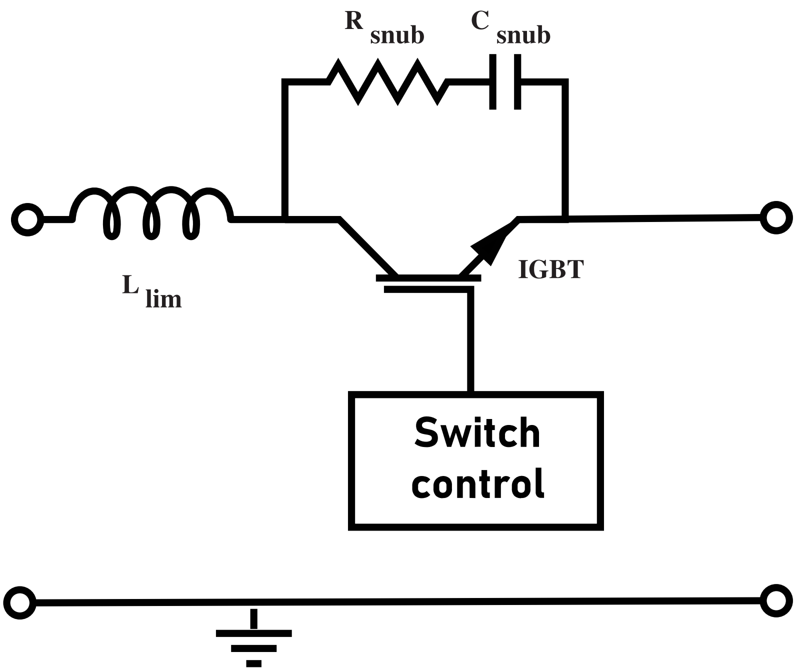

Figure A.2: The final circuit breaker design of a unidirectional circuit breaker with current limiter and snubber circuit

Table A.2: The values for the final design of the circuit breaker

Component	**Value**
Inductor	42 μH
Capacitor	40 μF
Resistor	3 Ω

Table A.3: Dimensions of the Toroidal Inductor

Dimension	**Value (cm)**
Inner Radius of Core	5.47
outer Radius of Core	8.84
Width of the Air Gap	1.10
Width of the Core	3.37

Table A.4: The mass of each component for the upscaled circuit breaker

Component	Mass (kg)
Thin film capacitor	1.92
Wire wound resistor	0.0178
Air core inductor	7.16
Solid state switch	1.4
Total mass	11

Table A.5: The failure rate of each component and the combined failure rate of the circuit breaker with a fuse

Component	Failure rate (Failures/Flight hour)
Thin film capacitor	$26.2 \cdot 10^{-9}$
Wire wound resistor	$18.9 \cdot 10^{-9}$
Permendur toroid core inductor	$0.69 \cdot 10^{-9}$
Solid state switch	$79.6 \cdot 10^{-9}$
Fuse	$228 \cdot 10^{-9}$
Total failure rate (without fuse)	$125.39 \cdot 10^{-9}$
Total failure rate (with fuse)	$285 \cdot 10^{-12}$

Bibliography

[1] Y. Wang, C. Zhang, C. Zhang, and L. Li, "Review of high-power-density and fault-tolerant design of propulsion motors for electric aircraft," *Energies*, vol. 16, no. 19, 2023, ISSN: 1996-1073. DOI: 10.3390/en16197015. [Online]. Available: https://www.mdpi.com/1996-1073/16/19/7015.

[2] E. Airlines, *Elysian airlines webpage*, https://www.elysianairlines.com/, Accessed: 2024-06-17.

[3] F. W. Tim ter Horst Mark Imhof, *Design & reliability assessment of aea propulsion grid*, 2024.

[4] an EnerSys company, "High altitude derating factors for electrical systems," 2024. [Online]. Available: https://atl.my.site.com/OutbackKnowledgeCentre/s/article/High-altitude-derating-factors-for-electrical-systems.

[5] *Highly insulated module with trench/fieldstop igbt3 and emitter controlled 3 diode*, FZ750R65KE3, infineon, 2021. [Online]. Available: https://www.infineon.com/dgdl/Infineon-FZ750R65KE3-DataSheet-v01_10-EN.pdf?fileId=db3a304325afd6e00126461fd3936974.

[6] V. Raghavendra I, B. S. Naik, T. Sreekanth, and A. Chub, "Controlled bidirectional dc circuit breaker with zero negative current for high load shift applications," *IEEE Transactions on Industry Applications*, vol. 58, no. 6, pp. 6942–6951, 2022. DOI: 10.1109/TIA.2022.3193345.

[7] I. Venkata Raghavendra, S. N. Banavath, C. Muhammed Ajmal, and A. Ray, "Modular bidirectional solid-state dc circuit breaker for next-generation electric aircrafts," *IEEE Journal of Emerging and Selected Topics in Power Electronics*, vol. 10, no. 5, pp. 5486–5497, 2022, Cited by: 17. DOI: 10.1109/JESTPE.2022.3176929. [Online]. Available: https://www.scopus.com/inward/record.uri?eid=2-s2.0-85130796680&doi=10.1109%2fJESTPE.2022.3176929&partnerID=40&md5=eae7683ccfc802329e722311230f27b6.

[8] U. Mehrotra, B. Ballard, T.-H. Cheng, B. J. Baliga, S. Bhattacharya, and D. C. Hopkins, "Optimized highly efficient sscb using organic substrate packaging for electric vehicle applications," *2020 IEEE Transportation Electrification Conference & Expo (ITEC)*, Jun. 2020. DOI: 10.1109/itec48692.2020.9161539. [Online]. Available: https://www.osti.gov/biblio/2324648.

[9] S. Kamtip and K. Bhumkittipich, "Comparison between mechanical circuit breaker and solid state circuit breaker under abnormal conditions for low voltage systems," in *2015 18th International Conference on Electrical Machines and Systems (ICEMS)*, 2015, pp. 1091–1096. DOI: 10.1109/ICEMS.2015.7385200.

[10] H. Schefer, L. Fauth, T. H. Kopp, R. Mallwitz, J. Friebe, and M. Kurrat, "Discussion on electric power supply systems for all electric aircraft," *IEEE Access*, vol. 8, pp. 84 188–84 216, 2020, Cited by: 109; All Open Access, Gold Open Access, Green Open Access. DOI: 10.1109/ACCESS.2020.2991804. [Online]. Available: https://www.scopus.com/inward/record.uri?eid=2-s2.0-85084918886&doi=10.1109%2fACCESS.2020.2991804&partnerID=40&md5=cd75eb8f061ffd3b5b58d8e36035c146.

[11] P. Suntharalingam and A. Baronian, "Solid state circuit breaker design with discrete sic mosfet's for aircraft electrification application," in *2021 IEEE Energy Conversion Congress and Exposition (ECCE)*, 2021, pp. 613–617. DOI: 10.1109/ECCE47101.2021.9595794.

[12] H. Bavishi, M. D'Arpino, P. Ramesh, Y. Guezennec, and I. Colbert, "Comparative analysis of protection systems for dc power distribution in electrified vehicles," 2022, Cited by: 0, 2022. DOI: 10.4271/2022-01-0135. [Online]. Available: https://www.scopus.com/inward/record.uri?eid=2-s2.0-85128007581&doi=10.4271%2f2022-01-0135&partnerID=40&md5=2f76a642ff2c36144c5b28d1a02a900b.

[13] M. Armstrong, M. Blackwelder, A. Bollman, *et al.*, "Architecture, voltage, and components for a turboelectric distributed propulsion electric grid," Jan. 2015.

[14] R. Mehl and P. Meckler, "Comparison of advantages and disadvantages of electronic and mechanical protection systems for higher voltage dc 400 v," Cited by: 9, vol. 2013-October, 2013. [Online]. Available: https://www.scopus.com/inward/record.uri?eid=2-s2.0-84941119787&partnerID=40&md5=096773862ad7c0126457694e9b43d29a.

[15] R. Boudreaux and R. Nelms, "A comparison of mosfets, igbts, and mcts for solid state circuit breakers," in *Proceedings of Applied Power Electronics Conference. APEC '96*, vol. 1, 1996, 227–233 vol.1. DOI: 10.1109/APEC.1996.500447.

[16] Y. He, C. Xu, Y. Li, I. Peng, and F. Z., "A survey of hybrid circuit breakers: Component-level insights to system-wide integration," *IEEE Open Journal of Power Electronics*, pp. 1–23, 2024, Cited by: 0. DOI: 10.1109/OJPEL.2024.3381000. [Online]. Available: https://www.scopus.com/inward/record.uri?eid=2-s2.0-85189162414&doi=10.1109%2fOJPEL.2024.3381000&partnerID=40&md5=bfcf6fee1e866562df78db7577a76001.

[17] A. Fayyaz, M. U. Ortiz, Z. Wang, T. Yang, and P. Wheeler, "Paralleling of transient overvoltage protection elements within high power dc solid-state circuit breaker (sscb) for electric/hybrid-electric aircraft," Cited by: 1, 2022. DOI: 10.1109/WiPDAEurope55971.2022.9936092. [Online]. Available: https://www.scopus.com/inward/record.uri?eid=2-s2.0-85142510257&doi=10.1109%2fWiPDAEurope55971.2022.9936092&partnerID=40&md5=e4c51d04962aa3f8db194aede09215c6.

[18] A. R. Figueiredo Bento, F. Bento, and A. J. Marques Cardoso, "A novel dc circuit breaker with an absorbing branch based on tvs diodes," in *2023 IEEE Fifth International Conference on DC Microgrids (ICDCM)*, vol. Single, 2023, pp. 1–5. DOI: 10.1109/ICDCM54452.2023.10433588.

[19] X. Song, Y. Du, and P. Cairoli, "Survey and experimental evaluation of voltage clamping components for solid state circuit breakers," in *2021 IEEE Applied Power Electronics Conference and Exposition (APEC)*, 2021, pp. 401–406. DOI: 10.1109/APEC42165.2021.9487424.

[20] X. Song, Y. Du, and P. Cairoli, "Survey and experimental evaluation of voltage clamping components for solid state circuit breakers," in *2021 IEEE Applied Power Electronics Conference and Exposition (APEC)*, 2021, pp. 401–406. DOI: 10.1109/APEC42165.2021.9487424.

[21] G. Dorj and L. Li, "Data mining applications in healthcare," *Procedia Computer Science*, vol. 72, pp. 797–804, 2015, ISSN: 1877-0509. DOI: 10.1016/j.procs.2015.12.196. [Online]. Available: https://www.sciencedirect.com/science/article/pii/S1876610215021372.

[22] X. Pei, A. C. Smith, and M. Barnes, "Superconducting fault current limiters for hvdc systems," *Energy Procedia*, vol. 80, pp. 47–55, 2015, 12th Deep Sea Offshore Wind R & D Conference, EERA DeepWind'2015, ISSN: 1876-6102. DOI: https://doi.org/10.1016/j.egypro.2015.11.405. [Online]. Available: https://www.sciencedirect.com/science/article/pii/S1876610215021372.

[23] *Piezo microactuator driver with boost regulator*, LT3469, Linear Technology, 2003. [Online]. Available: https://4donline.ihs.com/images/VipMasterIC/IC/LITC/LITCS09455/LITCS09455-1.pdf?hkey=52A5661711E402568146F3353EA87419.

[24] *Fast, robust, dual-channel, functional and reinforced isolated mosfet gate-driver with accurate and stable timing*, EiceDRIVER™ 2EDi product family, infineon, 2018. [Online]. Available: https://4donline.ihs.com/images/VipMasterIC/IC/INFN/INFN-S-A0006623190/INFN-S-A0006623190-1.pdf?hkey=6D3A4C79FDBF58556ACFDE234799DDF0.

[25] *Film capacitors - power electronic capacitors*, B25620C1706K981*, TDK, 2022. [Online]. Available: https://product.tdk.com/system/files/dam/doc/product/capacitor/film/power/data_sheet/20/50/ds/b2562_.pdf.

[26] E. ToolBox, *Permeability*, https://www.engineeringtoolbox.com/permeability-d_1923.html, Accessed: 2024-06-21, 2024. [Online]. Available: https://www.engineeringtoolbox.com/permeability-d_1923.html.

[27] M. A. Laughton and D. J. Warne, *Electrical Engineer's Reference Book*, 16th. Oxford, UK: Newnes, 2003.

[28] P. Milczanowski, *Density*, https://web.fscj.edu/Milczanowski/psc/lect/Ch4/slide6.htm, Accessed: 2024-06-21, 2024. [Online]. Available: https://web.fscj.edu/Milczanowski/psc/lect/Ch4/slide6.htm.

[29] T. Corporation, *Mn-zn ferrite material characteristics*, https://product.tdk.com/system/files/dam/doc/product/ferrite/ferrite/ferrite-core/catalog/ferrite_mn-zn_material_characteristics_en.pdf, Accessed: 2024-06-21, 2024. [Online]. Available: https://product.tdk.com/system/files/dam/doc/product/ferrite/ferrite/ferrite-core/catalog/ferrite_mn-zn_material_characteristics_en.pdf.

[30] S. Maniktala, "Chapter 2 - dc–dc converter design and magnetics," in *Switching Power Supplies A - Z (Second Edition)*, S. Maniktala, Ed., Second Edition, Oxford: Newnes, 2012, pp. 61–121, ISBN: 978-0-12-386533-5. DOI: https://doi.org/10.1016/B978-0-12-386533-5.00002-4. [Online]. Available: https://www.sciencedirect.com/science/article/pii/B9780123865335000024.

[31] I. Won, D. Keiswetter, and T. Bell, "Electromagnetic induction spectroscopy for clearing landmines," *IEEE Transactions on Geoscience and Remote Sensing*, vol. 39, no. 4, pp. 703–709, 2001. DOI: 10.1109/36.917876.

[32] A. Eschenfelder, "Chapter 6 amorphous films for bubbles," in ser. Handbook of Ferromagnetic Materials, vol. 2, Elsevier, 1980, pp. 168–170. DOI: https://doi.org/10.1016/S1574-9304(05)80107-5. [Online]. Available: https://www.sciencedirect.com/science/article/pii/S1574930405801075.

[33] ScienceDirect, *Copper (cu)*, Accessed: 2024-06-14, 2024. [Online]. Available: https://www.sciencedirect.com/topics/nursing-and-health-professions/copper.

[34] PowerStream, *American wire gauge chart and awg electrical current load limits*, Accessed: 2024-06-14, 2024. [Online]. Available: https://www.powerstream.com/Wire_Size.htm.

[35] L. Learning, *Inductance*, Accessed: 2024-06-14, 2024. [Online]. Available: https://courses.lumenlearning.com/suny-physics/chapter/23-9-inductance/.

[36] L. EETech Group, "Film capacitor," 2024. [Online]. Available: https://eepower.com/capacitor-guide/types/film-capacitor/#.

[37] OpenStax, "Work and kinetic energy," 2016. [Online]. Available: https://pressbooks.online.ucf.edu/phy2048tjb/chapter/power/.

[38] *High energy wirewound*, 35J1R5, Ohmite, 2022. [Online]. Available: https://www.ohmite.com/assets/docs/30%20Series%20Datasheet%20-%20Revised.pdf.

[39] SICT, "Density," 2020. [Online]. Available: https://ceramique-technique.com/en/properties/density#:~:text=according%20to%20the%20reference%20system,plastics%20but%20lighter%20than%20steels..

[40] *Military handbook, reliability predication of electronic equipment*. Department of defense Washington DC, 1991.

[41] *Circuit Breaker Operating Temperatures*, Schneider Electric Product Information, 2024. [Online]. Available: https://www.productinfo.schneider-electric.com/0600db1603cboptemps/0600db1603-circuit-breaker-operating-temperatures/0600DB1603%20Circuit%20Breaker%20Operating%20Temperatures/English/0600DB1603%20Circuit%20Breaker%20Operating%20Temperatures_0000362832.xml/$/Introduction-98EEE9A4.

[42] I. Galaxy Wire & Cable, *Conductor options for custom wire & cable*, https://www.galaxywire.com/custom-wire-cable/conductor-options/, Accessed: 2024-06-21, 2024. [Online]. Available: https://www.galaxywire.com/custom-wire-cable/conductor-options/.

[43] S. Yang, A. Bryant, P. Mawby, D. Xiang, L. Ran, and P. Tavner, "An industry-based survey of reliability in power electronic converters," *Industry Applications, IEEE Transactions on*, vol. 47, pp. 1441–1451, Jul. 2011. DOI: 10.1109/TIA.2011.2124436.

[44] ABB, "Application note 5sya 2042," ABB, Tech. Rep., Jun. 2019. [Online]. Available: https://library.e.abb.com/public/9cb3f71fafea4542b8c576555a29930a/ABB_Application%20Note%205SYA%202042_062019.pdf?x-sign=UtXTEMNpuUrOPPtq2g74muwsvzOck

[45] J. C. G. G. Campetelli and G. Zamanillo, "The reliability of high breaking capacity fuse," in *CIRED 1999 - 14th International Conference on Electricity Distribution*, 1999, 1_5. [Online]. Available: http://www.cired.net/publications/cired1999/papers/1/1_5.pdf.